Spintronic Terahertz Emitters: Status and Prospects from a Materials Perspective

DOI:
10.1063/5.0057511

Document Version
Accepted author manuscript

Spintronic Terahertz Emitters: Status and Prospects from a Materials Perspective

Charlotte Bull,[1,2] Simmone M. Hewett,[1] Ruidong Ji,[1] Cheng-Han Lin,[1] Thomas Thomson,[2] Darren M. Graham,[1,3] and Paul W. Nutter[2, a)]

[1)]*Department of Physics and Astronomy & Photon Science Institute, The University of Manchester, Oxford Road, Manchester M13 9PL, UK*

[2)]*Nano Engineering & Spintronic Technologies Group, Department of Computer Science, The University of Manchester, Oxford Road, Manchester M13 9PL, UK.*

[3)]*The Cockcroft Institute, Sci-Tech Daresbury, Keckwick Lane, Daresbury, Warrington WA4 4AD, UK*

(Dated: 23 July 2021)

Spintronic terahertz (THz) emitters, consisting of ferromagnetic (FM)/non-magnetic (NM) thin films, have demonstrated remarkable potential for use in THz time-domain spectroscopy and its exploitation in scientific and industrial applications. Since the discovery that novel FM/NM heterostructures can be utilized as sources of THz radiation, researchers have endeavoured to find the optimum combination of materials to produce idealized spintronic emitters capable of generating pulses of THz radiation over a large spectral bandwidth. In the last decade, researchers have investigated the influence of a wide range of material properties, including the choice of materials and thicknesses of the layers, the quality of the FM/NM interface, and the stack geometry upon the emission of THz radiation. It has been found that particular combinations of these properties have greatly improved the amplitude and bandwidth of the emitted THz pulse. Significantly, studying the material properties of spintronic THz emitters has increased the understanding of the spin-to-charge current conversion processes involved in the generation of THz radiation. Ultimately, this has facilitated the development of spintronic heterostructures that can emit THz radiation without the application of an external magnetic field. In this review, we present a comprehensive overview of the experimental and theoretical findings that have led to the development of spintronic THz emitters which hold promise for use in a wide range of THz applications. We summarise the current understanding of the mechanisms that contribute to the emission of THz radiation from the spintronic heterostructures, and explore how the material properties contribute to the emission process.

[a)]Electronic mail: P.Nutter@manchester.ac.uk

I. INTRODUCTION TO SUB-PICOSECOND TERAHERTZ EMITTERS

Since the first development of terahertz time-domain spectroscopy (THz-TDS) in the 1980s,[1,2] the technique has found application in numerous areas of science and engineering. Today, it is being utilized for the characterization of materials,[3–5] for industrial process monitoring,[6–8] and to identify chemical compounds.[9–11] While all terahertz time-domain spectrometers utilize femtosecond pulses of laser light to create a sub-picosecond transient current or electronic polarization in order to generate pulses of broadband terahertz (THz) frequency radiation, there are a plethora of different materials employed for the THz generation process. THz emitters include photoconductive antennas (employing GaAs[12–21] or InGaAs[22–24]), organic and inorganic nonlinear crystals (ZnTe,[25–32] GaP,[33–35] $LiNbO_3$,[36,37] DAST,[38,39] DSTMS,[39–42] OH1,[39,41,43] and BNA[44]), and recently, air plasma,[45–49] liquids[50] and metamaterials.[51] The reason for the large diversity of THz emitters employed is because not one particular source offers all of the desirable characteristics, including: a high THz electric-field amplitude, a broad spectral bandwidth, a gapless spectral coverage, and the requirement of only modest nano-joule laser pulse energies to excite the emitter. The table shown in Figure 1 compares the characteristics of commonly used THz emitters in THz-TDS.

Photoconductive antennas (PCAs), which consist of a gap typically several microns wide between metal contacts deposited onto a photoconductive semiconductor substrate, generate THz radiation by accelerating photo-excited carriers using an externally applied bias field. For an overview of THz PCA technology, see the comprehensive reviews by Burforda & El-Shenawee[52] and Isgandarov *et al.*[53] The drawbacks with PCAs include: the high fabrication cost associated with microlithography, the added complexity of the requirement for an external bias voltage, and the difficulty in scaling to higher electric-field amplitudes. This difficulty arises from the limit placed on optical excitation fluences by the damage threshold of the photoconductive material. In addition, the polar semiconductors commonly used have strong optical phonon resonances across the THz spectral region, preventing a gapless spectral coverage. Here, a gapless coverage is particularly desirable due to the large number of important electronic and vibrational modes within the THz spectral region. Nevertheless, emission spectra extending up to 20 THz and 30 THz have been demonstrated using semi-insulating (SI)-[15] and low-temperature grown (LTG)-[16] GaAs photoconductive antennas, respectively. A 70 THz bandwidth was also recently demonstrated using a non-polar Ge photoconductive antenna.[54] In the 1990s, an electric-field strength of 150 $\mathrm{kV\,cm^{-1}}$ was

reported for a large-area LTG-GaAs PCA[19] and 350 kV cm^{-1} for a large-area SI–GaAs PCA.[20] However, Hattori *et al.*[21] highlighted that the estimation of electric-field strength from the pulse energy measurements employed in[19,20] were indirect and unreliable. This is due to the finding that Hattori *et al.* were only able to achieve an electric-field strength of 5.7 kV cm^{-1} from a large-area SI–GaAs PCA with the same electrode spacing. Recently, a high electric-field strength has been realized in a large-area photoconductive THz array structure,[17] consisting of a thin LTG-GaAs active region transferred to an insulating substrate, with a reported value in excess of 120 kV cm^{-1}.

Nonlinear crystals, such as inorganic ZnTe and GaP, and organic DAST and DSTMS, are commonly used for THz generation in THz-TDS due to their large nonlinear susceptibilities. In such crystals, the driving laser pulse generates a transient polarization which in turn emits a broadband THz pulse. The main drawback with inorganic, nonlinear crystals is the requirement to match the optical group velocity of the driving laser pulse to the THz phase velocity for efficiency generation. This requirement restricts the photoexcitation wavelength that may be used and limits the spectral bandwidth of the source. As these nonlinear crystals are polar in nature, they also suffer from optical phonons, which produce a highly absorbing Reststrahlen band within the THz spectral region. This absorption either limits the bandwidth of the emitted THz pulse or produces a gap within the spectral content of the source. By using a thin crystal or a thin film to minimize the optical group- and THz phase-velocity walk-off, a 30 μm thick (110)-cut ZnTe crystal and a 10 μm thick (111)-grown ZnTe film have produced broadband emission with spectral content up to 40 THz.[26,27] However, these emission spectra demonstrate significant gaps across the spectrum. $LiNbO_3$ inorganic crystals are often used for the generation of high fields,[36,37] with electric-field strengths of up to 4.0 MV cm^{-1} being reported, although $LiNbO_3$ suffers from requiring a complex tilted-pulse-front-pumping scheme for velocity matching.

Organic, nonlinear crystals have, in contrast, achieved some of the highest reported electric-field strengths. A value of 62 MV cm^{-1} has been reported for the non-ionic polyene crystal OH1,[41] and a value of 83 MV cm^{-1} has been reported for the stilbazolium salt DSTMS.[41] However, the spectra emitted from organic crystals are affected by a large number of vibrational absorption bands,[38,40] preventing a gapless spectral coverage over the 0.1-10 THz region. For a thorough review of organic crystals see the work of Jazbinsek *et al.*[55] and for a comprehensive comparison of high-field THz sources see the review by Fülöp *et al.*[56].

The continued desire for THz emitters that can generate an ultra-broadband THz spectrum, covering the far- and mid-infrared spectral region with gapless coverage, has been recently re-

alised by using air-plasma generation. Such THz sources have demonstrated a bandwidth of more than 100 THz,[48,49] limited only by the pulse duration of the photo-exciting laser, and electric field strengths of 400 kV cm^{-1}.[47] However, the key drawback with air-plasma sources is the requirement for high photoexcitation pulse energies (on the order of 100's μJ) for the generation of the plasma. Furthermore, air-plasma generation can also suffer with large shot-to-shot pulse fluctuations.

A promising new class of THz emitters have recently emerged that have already demonstrated a gapless broadband emission reaching up to 30 THz.[57] They require photoexcitation with only nano-joule energy pulses,[57] are cheap to manufacture, and have demonstrated scalability for the generation of higher THz field amplitudes (up to 300 kV cm^{-1}).[58] They also appear to be independent of the photo-excitation wavelength.[59] These so-called spintronic, or spin-based emitters, consist of bilayers of ferromagnetic (FM) and non-magnetic (NM) heavy metal thin films. The mechanism for THz emission, as shown in Figure 2, relies on the generation a spin current, $\boldsymbol{j}_s$, in the FM layer and subsequent conversion of this to a transient charge current, $\boldsymbol{j}_c$, in the NM layer. Consequently, such emitters are referred to as spintronic, or spin-based, emitters.

Research to date has focused predominately upon maximizing the emission amplitude of the THz pulse by investigating a range of material combinations[57,60–63] and film thicknesses[57,60,64] for the FM/NM bilayer structure. So far, THz pulses with the highest electric field amplitudes have been observed when using CoFeB as the FM material in combination with a NM material that exhibits a large spin-orbit coupling, such as Pt.[57,58,60–62,65] A detailed review of material combinations and thicknesses can be found in section II.A and II.B. Further approaches investigated for increasing the amplitude of the emitted pulse include the use of multilayer[66] and trilayer films (W/CoFeB/Pt),[57,58,61] which take advantage of the flow of the spin current in both directions through the FM thin film to boost the spin-to-charge conversion efficiency.[57] Changing the material properties by post deposition annealing has been shown to influence the amplitude of the THz pulse when using a CoFeB FM layer.[64,67] In addition, the observation of emission of pulses of THz radiation from spintronic heterostructures with broken interfaces[68,69], detailed in section III, has enthused a research drive to understand the influence of interfacial properties upon the interfacial spin-to-charge current conversion mechanism.[70] Whilst it has been established that particular combinations of FM/NM materials can maximize the emitted THz electric field amplitude, a detailed understanding of the role that interfaces and material properties contribute to the generation process of THz frequency radiation in these systems is less well understood. In particular, the ef-

fects of varying the material properties such as the roughness, crystal structure, and strain from the substrate have not been widely reported. Further research will be necessary to inform the design of emitters that the offer optimum performance required for scientific and industrial applications of THz-TDS. In this review, we discuss experimental and theoretical findings which have led to the development of spintronic THz emitters. We begin to answer the vital question - what combination of materials and properties are required to produce an emitter which can generate pulses of THz radiation with a large spectral bandwidth and high electric field strength? By comparing ideas from literature, we discuss possible mechanisms that contribute to the THz emission from spintronic sources, and highlight how material and interfacial properties of the system contribute to the generation and emission process.

A. Background: Ultrafast magnetism and spin dynamics

The physical processes associated with illuminating metallic thin films using picosecond laser pulses were predicted almost 50 years ago by Anisimov *et al.* who developed a numerical model for the emission of electrons from a metallic surface.[71] This model was derived from the two competing phenomena: 1) the photoelectric effect, and 2) the heating of the metallic surface, resulting in thermionic emission. At the time, these phenomena had been extensively investigated in metals using millisecond and nanosecond pulses[72–75] allowing the photoelectric effect and the thermionic effect to be separated.[76] However, the separation of these effects for picosecond pulses was complex as the pulse duration was shorter than the characteristic time for the transfer of energy between electrons and the lattice in metals.[71] Considering this, Anisimov *et al.* predicted an additional increase in electron temperature, T_e, with respect to the lattice temperature, T_i, of metals subjected to ultrafast heating, which was experimentally observed 8 years later by Eesley.[77] In order to observe non-equilibrium electron heating above the lattice temperature, Eesley used picosecond laser pulses to excite electrons in a 400 nm thick Cu film and to probe the thermally induced reflectivity, $\Delta R/R$, at normal incidence from the film surface in a non-collinear pump-probe configuration. During the 40 ps delay between the initial heating pulses (with photon energy 1.92 eV) and the successive probe pulses (with tunable photon energies between 2.03-2.17 eV), Cu reflectivity transients were observed to have both a fast and a slow decay component, with the slow decay having a lifetime of approximately 200 ps, as shown in Figure 3. The rapid change in $\Delta R/R$ on a timescale of less than 15 ps was attributed to direct electron heating and cooling.[77]

In resolving the Fermi level smearing components of $\Delta R/R$ (to extract T_e) and comparing these to the photon energies of the probe pulses, it was implied that T_e exceeded T_i during the heating pulse.[77] Due to the limited resolution of a picosecond time frame, the hot electron decay time τ_e, could not be determined.[77] However Eesley's experiments confirmed that non-equilibrium heating of electrons was taking place in copper.

Following Eesley's work, picosecond laser pump-probe experiments were performed on a range of metals, including W, Ag, Au and Sn, in which the non-equilibrium heating of electrons was observed.[78–80] It was additionally shown by Agranat *et al.*[79] that the deviation of T_e from T_i could be substantial, reaching $\sim$4 x10^3 K in Ag.[79] Subsequently, the first picosecond pulsed laser experiments performed on ferromagnetic materials were conducted by Agranat *et al.* on Ni films,[81] and Vaterlaus *et al.* on Fe films[80] to investigate ultrafast, laser-induced magnetization dynamics. In particular, the characteristic time required to establish thermal equilibrium between the heated lattice and the spin system of ferromagnets, known as the spin-lattice relaxation time τ_{is}, was of technological interest at the time for determining speeds attainable in Curie-point writing for magneto-optical recording.[82] Changes in the magnetization of 50-100 nm thick Ni films were therefore measured using the magneto-optical Kerr effect[83] after applying single, picosecond or nanosecond laser pulses with fluence 100 mJ cm^{-2}. It was found that heating the 50 nm Ni film using pulses of duration τ_p = 5-20 ps did not produce observable changes to the magnetization of Ni. However, using pulses of duration τ_p = 40 ns resulted in demagnetization of the heated section of the film as T_i was able to reach temperatures approximately 2.5 times higher than the Curie temperature of Ni (T_C = 631 K).[81] The spin-lattice relaxation time for Ni, within the vicinity of T_C, was determined to be within the interval 1 ns < τ_{is} < 40 ns.[81] A similar behavior was observed in 5 mm thick Fe films by Vaterlaus *et al.*,[80] who conducted a spin-polarized photoemission experiment using a pulsed dye laser (with photon energy 2.15 eV) to illuminate the films with τ_p = 30 ps and 20 ns. The spin polarization of the photoelectrons emitted from the film remained constant over the duration of the 30 ps pulse, even as the laser fluence was increased to the value necessary to melt the Fe lattice, approximately 90 mJ cm^{-2}. In contrast, during the 20 ns pulse, a decrease in polarization was observed for both a solid and a liquid Fe film, consistent with a demagnetization of the Fe at the point where $T_i \geq T_C$.[80] It was therefore concluded that Fe could not be demagnetized within the duration of a 30 ps laser pulse due to τ_{is} > 30 ps.[80] In following year, Vaterlaus *et al.* successfully measured the spin-lattice relaxation time in ferromagnetic Gd.[82] To raise the temperature of the lattice, the 5 nm thick Gd film was illuminated using a laser pulse of 10 ns dura-

tion and photon energy of 2.15 eV, which was less than the photothreshold of the sample, so as not to emit photoelectrons. Simultaneously, a synchronized laser pulse of 60 ps duration and photon energy of 3.2 eV was used to induce emission of electrons from the Gd, allowing the measurement of the time resolved spin-polarized photoemission.[82] The variation of magnetization during the ns heating pulse was determined as a function of time, giving the characteristic time for the heat transfer from the lattice to the spin system of ferromagnetic Gd to be $\tau_{is} = 100 \pm 80$ ps.[82]

Until the beginning of the 1980s, ultrafast lasers were limited to the picosecond time resolution. However, by the mid 1980s, the development of high-repetition rate sources[84–86] made it possible to investigate non-equilibrium electron heating of metals in the femtosecond regime. Experiments undertaken in this regime have enabled critical temperature dynamics to be studied using femtosecond thermomodulation. This is a particularly powerful technique which separates electronic processes from phonon or lattice heating effects.[87] The first, direct measurement of the time taken, τ_e, for hot electrons to decay from a maximum to equilibrium temperature in the system was reported independently by Schoenlein *et al.* in 100 nm thick Au films[87] and by Elsayed-Ali *et al.* in 20 nm thick Cu films.[88] In both pump-probe experiments, high power femtosecond duration pulses were generated by a colliding pulse mode (CPM) locked laser (with photon energy 2.0 eV) and intensified using a copper vapor laser (CVL) amplifier.[87,88] Amplified pulses were focussed into an ethylene glycol cell to generate continuum broadband pulses. Such pulses were subsequently used to probe the reflectivities of Au (for wavelength range 580-450 nm) and Cu (for wavelength range 560-640 nm) as a function of time, enabling the electron decay time to be resolved in Au, $\tau_e \approx$ 2-3 ps,[87] and in Cu, $\tau_e \approx$ 1-4 ps.[88] A positive correlation was observed between the heating pulse fluence (1.4-11.4 mJ cm^{-2}) and the electron decay time in Cu. Elsayed-Ali *et al.* proposed that higher pulse fluences increased the temperature difference between T_e and T_i, hence, the increase in electron decay time was attributed to the greater number of electron-phonon collisions necessary for the Cu film to thermalise.[88]

In 1996, Beaurepaire *et al.* performed the first femtosecond pulsed laser experiments on ferromagnetic Ni allowing demagnetisation processes to be measured.[89] In contrast to previous experiments on ferromagnetic materials,[80–82] Beaurepaire *et al.* used a time scale in which the electron-spin and spin-lattice relaxation mechanisms could be resolved independently.[89] The 20 nm thick Ni films were illuminated using a CPM locked laser with pulse duration $\tau_p = 60$ fs and wavelength 620 nm (amplified using a CVL) in order to induce and measure the electronic thermalisation process. Simultaneously, the spin dynamics of Ni were measured using the time resolved longitudinal

Magneto-Optical Kerr Effect (MOKE),[83] where a full magnetic hysteresis loop was recorded prior to illumination via the pump beam, and for each delay, Δt, between the pump and probe pulse.[89] It was discovered that when the film was illuminated by a pump of fluence of 7 mJ cm^{-2}, a striking decrease in the magnetization of the Ni could be observed at zero field, M_r, which occurred within Δt = 2 ps, followed by a relaxation to a plateau, shown in Figure 4(a). The magnetization of the film decreased rapidly during the first picosecond which indicated a fast increase of the spin temperature, T_S, of Ni.[89] However, from the calculation of electron and spin dynamics, T_e, T_S and T_i, of the film over a range Δt = 0-5 ps, it was demonstrated that they behave differently after the first few picoseconds, shown in Figure 4(b). In the intervening years since the seminal work by Beaurepaire,[89] a significant research effort has been devoted to understanding the physical origins of this effect in a variety of materials. However, the microscopic mechanism by which these effects occur have yet to be unambiguously established.[90–94] In conclusion, the remarkable discovery that the demagnetization of Ni could be induced using femtosecond pulses of laser light[89] challenged the fundamental understanding of magnetism at the time, stimulating research interest in the ultrafast processes occurring in ferromagnetic materials.

B. Current understanding: Emission process from a FM/NM bilayer

An increased understanding of the all-optical generation of spin currents using ultrafast laser pulses[95–97] and of spin transport processes in ferromagnetic materials[98–100] has led to the development of ultrafast, THz spintronic emitters. Novel spintronic THz emitters, designed by Kampfrath *et al.* in 2013,[101] consisted of ferromagnetic (FM)/non-magnetic (NM) bilayers, as shown in Figure 2. Following the first experimental demonstration of the all-optical generation and detection of sub-picosecond, oscillating spin current,[95] laser pulses with femtosecond duration have been used to trigger the picosecond excitation process in spintronic emitters.[57,61,64,101,102] Illuminating a spintronic emitter with intense, fs laser pulses creates excited, hot electrons in the ferromagnetic film which undergo a superdiffusive spin transport process to the NM layer.[91,96,97,103] The superdiffusive process describes the motion of hot electrons, which is ballistic over short excitation times, and diffusive (governed by Brownian motion) over longer excitation times.[103] In 2010, it was shown theoretically by Battiato *et al.*,[103] and demonstrated experimentally a year later by Melnikov *et al.*,[96] that the superdiffusive spin transport process could explain the mechanism of ultrafast demagnetization observed in 3*d* ferromagnets. After the absorption of a photon, electrons

in the FM layer are excited from the *d* band to the *sp* bands above the Fermi level, increasing in mobility.[103] The asymmetry of the band structure gives rise to hot-electron lifetimes that are spin-dependent,[97] giving excited majority spins a longer mean free path than excited minority spins in the FM layer.[103] The subsequent depletion of majority spin carriers in the FM layer, causes a decrease in the net magnetization of the ferromagnet.[97,103]

Some studies have attributed the diffusive spin transport process to an ultrafast, spin-dependent Seebeck effect,[98,104,105] shown in Figure 5. Experimental work to determine the timescales of these ultra-fast processes indicates that the superdiffusive transport process and the ultrafast spin-dependent Seebeck effect occur over similar timescales of approximately 1 picosecond.[101,106] The spin-dependent Seebeck effect, which has been demonstrated in lateral spin valve structures,[107] refers to the generation of a spin current, induced by a temperature gradient, in a ferromagnet. This spin current is generated because in the ferromagnet, the Seebeck effect, which describes the generation of a potential difference (voltage) due to a temperature gradient,[108] is spin-dependent.[107] The spin-dependent scattering rates and densities of conduction electrons in the ferromagnet give rise to individual Seebeck coefficients, S, for spin-up (↑) and spin-down (↓) electrons.[108] Therefore, when subjected to a temperature gradient, ∇T, or consequently, a heat current, ∇Q, a spin current, $\mu_\uparrow$ - $\mu_\downarrow$, proportional to ∇T traverses the ferromagnet, where $\mu_\uparrow$ and $\mu_\downarrow$ are the electrochemical potentials for spin-up and spin-down electrons respectively.[108] ∇Q is conserved across the NM/FM interface, therefore ∇T is discontinuous between the ferromagnetic layer and the non-magnetic layer, as $Q = -k_{FM}\nabla T_{FM}$, where k_{FM} is the thermal conductivity of the ferromagnet.[107] As a result, the heat current induces a spin imbalance close to the interface proportional to $\mu_\uparrow$ - $\mu_\downarrow$. This spin accumulation relaxes in the FM and NM layers on the length scale of their spin-relaxation lengths λ_{FM} and λ_{NM}, respectively.[107]

The observation of thermally-driven spin injection across a FM/NM interface[91,107–109] has opened up the possibility of utilizing the spin-dependent Seebeck effect as an alternative to electrical spin injection techniques for spin-transfer-torque (STT) driven devices. In 2014, Choi *et al.*[98] demonstrated this concept experimentally in a Pt/FM_1/Cu/FM_2 heterostructure, as shown in Figure 6. In this work, an 800 fs laser pulse was used to create a heat current in the Pt layer which traverses the Pt/FM_1 interface.[98] This led to an ultrafast demagnetization of the FM_1 layer with perpendicular anisotropy, which was attributed to electron-magnon coupling.[98] Choi *et al.* report that differences in the temperatures of electrons and magnons in the rapidly heated FM_1 layer enabled the conversion of the demagnetization to a thermally-driven spin diffusive current,

which traversed across the FM_1/Cu interface. This thermally-driven current was then absorbed by the FM_2 layer, where a STT acting on the FM_2 layer led to the precession of the magnetic moment.[98] These findings have led to ongoing investigations of thermally-driven spin currents as a mechanism for diffusive spin transport in spintronic THz emitters.[57,58,106]

More recently, however, it has been shown by Rouzegar *et al.*[110] that the laser-induced spin transport in a FM/NM spintronic THz emitter arises from the same force that drives ultrafast demagnetization in a FM thin film.[110] This force is given by $\Delta\bar{\mu}_s = \mu_\uparrow - \mu_\downarrow$, and is referred to as a generalised spin voltage.[110] Rouzegar *et al.* report that $\Delta\bar{\mu}_s$ is caused by a pump-induced increase in the temperature of photoexcited electrons in the FM thin film which leads to a shift in $\mu_\uparrow$ and $\mu_\downarrow$ of majority- and minority- spin electrons in the FM layer, respectively. Alternatively to previous work,[98,104,105] Rouzegar *et al.* have explained their results, detailed in[110], without the assumption of a temperature difference between the FM and NM layer, or a temperature difference between the majority and minority electrons in the FM layer. Therefore, the authors report that the laser-induced spin transport in a FM/NM spintronic THz emitter is not the result of a spin-dependent Seebeck effect.[110]

While the mechanism driving the spin current is still under debate, it is widely accepted that a spin current, $\boldsymbol{j}_s$, with polarization, σ, diffuses across a FM/NM layer interface and is converted into an ultrafast charge current density, $\boldsymbol{j}_c$, in the NM layer via an inverse spin-Hall effect (ISHE).[99,100] It has been shown that the ISHE is driven by the spin-orbit interaction in the NM layer, which acts to deflect electrons travelling along the spatial direction of $\boldsymbol{j}_s$, aligned parallel or antiparallel to the direction of σ.[100] Consequently, electrons with opposing spins are deflected in opposite directions,[100] inducing a charge current density transverse to $\boldsymbol{j}_s$, as shown in Figure 2.

The charge current due to the ISHE, first measured experimentally in a NiFe/Pt bilayer by Saitoh *et al.*[100] and in the Al layer of a lateral spin valve by Valenzuela *et al.*[99] in 2006, can be expressed as,[101]

$$\boldsymbol{j}_c = \alpha_H \boldsymbol{j}_s \times \frac{\mathbf{M}}{|\mathbf{M}|} \tag{1}$$

where $\mathbf{M}$ denotes the magnetization in the FM layer, which is a function of the externally applied field, and α_H is the spin-Hall angle which characterises the electron deflection[101] and therefore the ISHE efficiency.[111] Due to their large spin-Hall angles, Pt and other metals with large spin-orbit coupling are chosen for the NM layer in spintronic THz emitters.[57,58,60–62,65,101]

The transverse charge current density, $\boldsymbol{j}_c = \alpha_H \boldsymbol{j}_s$, acts as a source of THz radiation in the NM

layer.[10157] This leads to the emission of a linearly polarized THz pulse, with an electric field direction perpendicular to the magnetization, **M**, of the FM layer[101] (shown in Figure 2). Due to the relationship between charge current and M shown in Eq. (1) emission only occurs when M is in-plane. If M is brought out-of-plane then this will result in no THz pulse being emitted. Throughout the literature an external magnetic field is applied to saturate the FM layer in-plane, thus maximising M and the corresponding THz output (see equation 1). However, the effect of operating at remanence has been investigated by Guo et al.[112] and Kampfrath et al.[101] Guo et al.[112] demonstrated THz emission from W/CoFeB/Pt trilayer emitters in the absence of an applied field, resulting in an emitted THz pulse with an amplitude/bandwidth comparable to a typical ZnTe emitter. Here, the sample was saturated along a known easy axis prior to the emission experiment taking place. Kampfrath et al. (see supplementary material for reference[101]) investigated field-free emission from an Fe/Au bilayer and found that the resulting emitted THz pulse was half the amplitude of that observed when an in-plane saturating magnetic field was applied; they ascribe the reduction in emission to the formation of randomly oriented magnetic domains. The polarization of the THz pulse is independent of the polarization of the laser pump pulse.[101] We direct the reader to references[105,110,113–115] which provide a more in-depth discussion of the underlying processes of THz emission from these systems.

The dependence of the polarization on **M** offers a unique potential to control the polarization profile of THz pulses,[102,113] as depicted in Figure 7, with potential applications in THz-driven electron-hole recollisions (for high-order-sideband generation),[116] ferroelectric domain switching[117] and rotatable polarization spectroscopy.[118] Furthermore, the ability to generate unique THz polarization profiles, demonstrated by Hibberd *et al.*,[102] could allow more complex modes, such as radial polarization,[119] to be obtained. Such modes offer high-efficiency coupling of THz radiation to cylindrical wire waveguides,[120] and when focused, could provide the strong longitudinal electric field component desired for THz-driven particle acceleration.

II. IMPACT OF MATERIAL CHOICES ON TERAHERTZ EMISSION

A significant body of work has been devoted to exploring the impact of different material combinations on the emission from spintronic THz emitters. Figure 8 provides a table that shows the number of papers published where the THz emission has been investigated for the different material combinations. Figure 8 demonstrates that a range of materials have been investigated for the

NM layer (layer 1), including topological insulators, semiconductors, and in some cases magnetic materials. These NM material choices are mapped against the range of magnetic materials that have been investigated for the magnetic (FM) layer (layer 2), which include ferromagnetic, ferrimagnetic and antiferromagnetic thin films. The colormap gives an indication of the number of papers that have been published for each material combination. Also shown is whether bilayer (red circle), trilayer (blue triangle), or multilayer structures (green square) have been investigated for each material combination. Additionally, Figure 8 shows a range of single layer magnetic materials from which THz emission has been observed, without the need for the NM layer. The impact of material choice on the THz emission is discussed in greater detail in the following sections. However, Figure 8 demonstrates that the use of a Pt NM layer in combination with a Co or CoFeB FM layer are the two popular avenues of exploration for spintronic THz emitters.

A. Optimization of FM/NM bilayer materials

In 2013, Kampfrath *et al.*[101] demonstrated that the temporal shape of the emitted THz pulse from a spintronic source can be manipulated using specifically designed FM/NM bilayers. In their work, 10 nm thick Fe films, evaporated onto glass substrates, were capped with a 2 nm thick layer of either Ru or Au to investigate how NM layers with a lower (Ru) or higher (Au) electron mobility could shape the emitted THz waveform. Using a 800 nm pump pulse with 20 fs duration to excite the Fe/Ru and Fe/Au bilayers, they observed significant differences in the emitted THz waveforms, as shown in Figure 9(a).

The amplitude spectrum, $|E_x(\omega)|$, of the Fe/Ru bilayer was found to cover a lower frequency range from $\omega/2\pi$ = 0.3 - 4 THz, whereas the emission spectrum from the Fe/Au bilayer extended to frequencies greater than 15 THz, as shown in Figure 9(b). This factor of four increase in bandwidth was attributed to the injection of hot electrons into the Au *sp* states, which have a high band velocity and greater mobility than Ru *d*-band states, which undergo more scattering due to a stronger electron-phonon coupling.[101] As a result of strong coupling, a significant spin accumulation of $\approx 0.2\,\mu_B$ per Ru atom was determined to occur in the Ru layer at an absorbed pump fluence of 1.3 mJ cm^{-2}. This was an order of magnitude greater than spin accumulation in the Au layer, leading to a much longer spin current pulse in the Fe/Ru bilayer.[101] These initial results demonstrated how the choice of NM material could influence the bandwidth of the THz emission from a FM/NM bilayer.

In agreement with Kampfrath *et al.*,[101] it has been found that larger THz electric field amplitudes have been obtained when using NM materials which have a high electron mobility[60–62] and exhibit a large spin-Hall conductivity,[57] such as Pt. The THz pulse amplitudes emitted from various NM materials coupled to $Co_{20}Fe_{60}B_{20}$ have been directly compared in a study by Seifert *et al.*[57] as shown in Figure 10.

The study by Seifert *et al.* showed that not only the amplitude of the THz waveform, but also the polarity of the THz electric field, correlates strongly with the amplitude and sign of the spin-Hall conductivity for the NM material chosen. Pt, for example, was found to produce pulses of THz radiation with waveform amplitudes an order of magnitude larger than Ta or Ir. However choosing W for the NM layer was found to produce pulse amplitudes of similar magnitude to Pd, but of opposite polarity.[57] Similar results were found by Wu *et al.*,[61] shown in Figure 11, from NM/Co/SiO_2 heterostructures excited by a fs laser with a pulse energy of 220 μJ. Choosing Pt as the NM material was found to produce THz pulses with the largest peak-to-peak amplitude of the six NM materials investigated: Pt, Ir, Gd, Ru, Ta and W, where the observed peak-to-peak amplitudes from Pt/Co/SiO_2 were approximately 2 times larger than W/Co/SiO_2 and Ir/Co/SiO_2, and an order of magnitude greater than Ta/Co/SiO_2, Ru/Co/SiO_2 and Gd/Co/SiO_2. The Ta/Co/SiO_2 and W/Co/SiO_2 heterostructures also generated THz waveforms of opposite polarity, indicating that the charge currents, $\boldsymbol{j}_c$, have a 180° phase shift in their oscillations.[61] Given that the electric field component of THz emission is dominated by $\boldsymbol{j}_c$ (induced by ISHE[57,101]), the sign change in the THz pulse was attributed to the sign change of α_H.[57,61]

More recently, an investigation of the emission of THz radiation from Al/Co heterostructures by Zhang *et al.*[121] has demonstrated that whilst maximum THz electric field amplitudes have been obtained when using heavy metals with a large-spin orbit coupling for the NM layer,[57,60–62,101] it may be worth revisiting light metals for cost-effective spintronic THz emitters. This is because despite the large difference between the spin-Hall angle of Al and Pt, where α_H = 0.03% and 3% (at 4.2 K) respectively,[61] the maximum THz electric field amplitude of Al (4 nm)/Co (3 nm)/SiO_2 was still found to be ∼34% that of Pt (4 nm)/Co (3 nm)/SiO_2. This recently measured response is greater than previously observed THz pulse amplitudes emitted from FM/NM heterostructures which have incorporated (heavy) NM metals with a lower spin-Hall conductivity, σ_H, such as Ta (3 nm) ($\sigma_H \approx$ -0.4 x10^5 Sm^{-1}) or Ir (3 nm) ($\sigma_H \approx$ 0.5 x10^5 Sm^{-1}), coupled to ferromagnetic $Co_{20}Fe_{60}B_{20}$ (3 nm).[57] These bilayers, shown in Figure 10, generated only 10% and 20%, respectively, of the maximum amplitude of THz radiation emitted from a CoFeB (3 nm)/Pt (3 nm)

bilayer, where $\sigma_H \approx 4.5$ x10^5 Sm^{-1} for Pt.[57] Similarly, the peak-to-peak THz pulse amplitudes emitted from Ta (4 nm)/Co (4 nm) heterostructures, investigated by Wu *et al.*,[61] reached only ∼8% of the maximum amplitude of THz radiation emitted from a Pt (4 nm)/Co (4 nm) heterostructure, as shown in Figure 11. However, curiously, in the comparative material study by Wu *et al.*,[61] the Ir (4 nm)/Co (4 nm) heterostructure combination generated a maximum peak-to-peak THz pulse amplitude of approximately 50% of the response from Pt (4 nm)/Co (4 nm) heterostructure, despite the fact that its spin-Hall conductivity is comparable to Ta.[57] This interesting response, along with the considerable THz electric field amplitude emitted from the Al (4 nm)/Co (3 nm) based heterostructure with respect to spin-Hall angle,[121] prompts further questions. It suggests that our current understanding of the generation mechanism of THz radiation in spintronic emitters is not complete. Whilst Zhang *et al.* were able to conclude that the strong emission of THz radiation from the Co (3 nm)/Al (4 nm) based heterostructure was a bulk effect occurring in the Al layer as a result of the ISHE, the physical origin was not clear, demonstrating the need for further experiments to uncover the underlying physics.[121]

One possibility for the unexpected range of THz electric field amplitudes emitted from varying NM materials could relate to the choice of FM material used for the heterostructure. The THz pulse amplitudes emitted from FM/NM heterostructures have been studied for a range of FM materials, including Fe, Co, Ni and their binary alloys.[57,60,122] As demonstrated by Seifert *et al.*[57] in Figure 12, FM materials (3 nm) coupled to Pt (3 nm) were found to emit THz pulses with similar amplitudes, with the exception of Ni. The alloy CoFeB, of the two studied compositions, produced the maximum THz pulse amplitude, whereas Ni yielded less than 20% of this maximum amplitude. This result has been hypothesised to be related to the low Curie temperature of Ni (627 K) in comparison to other FM materials (> 1000 K).[57]

In agreement with Seifert *et al.*,[57] Zhang *et al.*[60] have shown that in heterostructures consisting of Ta (3 nm)/Ru (5 nm)/FM (3 nm)/Ta (3 nm), where the FM material was CoFeB or CoFe, the resulting emitted THz pulse when using CoFeB yielded an approximately 9% greater peak-to-peak amplitude compared to CoFe. Whilst the reason for this small increase in THz pulse amplitude observed when using CoFeB for the FM material is not yet fully understood,[57,60] it has been hypothesised that it may be related to the higher spin polarization value of CoFeB (∼65%) in comparison to CoFe (∼47%).[60] This is because a higher spin polarization leads to the generation of a larger, superdiffusive spin current of hot electrons in the FM metal.

B. FM/NM material thickness dependence

The dependence of the emitted THz radiation on the thickness of the FM and NM layers in spintronic heterostructures have provoked significant research interest. It has been demonstrated theoretically that the total thickness, d_{tot}, of the heterostructure, along with the impedance, $Z(\omega)$, spin-Hall angle, α_H, and spin current, $\boldsymbol{j}_s$, can influence the emitted THz electric field amplitude, given by,[57]

$$E(\omega) = Z(\omega) e \int_0^{d_{tot}} \mathrm{dz}\ \alpha_H(z) \boldsymbol{j}_s(z, \omega). \tag{2}$$

Whilst equation (2) suggests that the THz electric field amplitude scales with d_{tot}, experimentally, the opposite trend has been observed.[57,60,61] It has been shown by Zhang *et al.*[60] that reducing the thickness of the non-magnetic, Pd layer from 10 nm to 5 nm in CoFeB (d_{CoFeB} nm)/Pd (d_{Pd} nm) based heterostructures, where d_{CoFeB} = 3-10 nm, increases the maximum amplitude of THz pulse emitted by $\sim$24%. Furthermore, decreasing the thickness of the ferromagnetic CoFeB layer from 20 nm to 3 nm, in the same CoFeB/Pd based heterostructures, increased the resulting THz pulse amplitude by $\sim$57%.[60] In $Co_{20}Fe_{60}B_{20}$/Pt bilayers, the total thickness, d_{tot}, dependence on the THz pulse amplitude has been further refined by Seifert *et al.*.[57] For bilayers with approximately equal NM and FM layer thicknesses, the amplitude of the THz pulse emitted was measured to increase with decreasing d_{tot}, peaking at d_{tot} = 4 nm, before rapidly decreasing for a smaller d_{tot},[57] as shown in Figure 13. In similar work, a FM layer thickness dependence study was carried out on Pt (4 nm)/Co (d_{Co} nm) and W (4 nm)/Co (d_{Co} nm) based heterostructures.[61] This showed that a peak THz pulse amplitude was measured when d_{Co} = 1-2 nm, before decreasing gradually with increasing FM layer thickness. Torosyan et al.[123] investigated the effect of layer thickness upon the emission of THz radiation from Fe (d_{Fe} nm)/Pt (d_{Pt} nm) bilayers. Here, the emission was measured for varying d_{Pt} and constant d_{Fe} = 12 nm and also for varying d_{Fe} and constant d_{Pt} = 3 nm. For both cases a sharp increase in the THz emission was observed with increasing film thickness, with the emission peaking for film thicknesses of 2 nm for Fe and 3 nm for Pt, with the THz emission shown to fall off as the film thickness is increased further. The overall increase in peak THz pulse amplitude with decreasing thickness (to a minimum d_{tot} value) has been attributed to the laser-induced spin diffusion length of majority spins[60,61] and most significantly, a photonic effect known as Fabry-Pérot resonance.[57,60] In detail, for a FM/NM bilayer structure, the metallic FM/substrate and NM/air interfaces act as two parallel reflecting surfaces, which effectively form a Fabry-Pérot cavity.[60] The length of this cavity is much smaller than the wavelength of the laser

pump pulse (calculated as 300 nm for an 800 nm pump pulse inside the metal film[60]) or the generated THz pulse, therefore reflections will remain in-phase and interfere constructively. This resonant enhancement of the pump and THz pulses is proposed to increase for shorter cavity lengths[57] as more reflections go back-and-forth through the film before the light field has decayed. Hence, the THz pulse amplitude increases with decreasing total bilayer film thickness, as shown in Figure 13. However, as the cavity reduces to a length smaller than some critical length, $d < d_c$, the reflection losses at the cavity interfaces dominate and no further benefit is gained from reducing the length to minimize the attenuation of the light field and maximise the number of reflections. The enhancement of the pump and THz light field is saturated at $d < d_c$ and can no longer compensate for the reducing emitter volume, hence the resulting sharp decrease in the THz pulse amplitude.[60]

In contrast to results observed by Zhang *et al.* for CoFeB/Pd heterostructures,[60] when studying the thickness dependence of Pt (d_{NM} nm)/Co (4 nm) and W (d_{NM} nm)/Co (4 nm) heterostructures, Wu *et al.*[61] observed that the maximum peak-to-peak THz pulse amplitude increased with increasing thickness of the NM layer, where d_{NM} = 2-10 nm.[61] For this case, the increasing amplitude of THz pulse emitted was attributed to an increase in the spin accumulation in the heterostructure, which resulted from increasing d_{NM}.[61] Interestingly, this result agrees with (2), as this relation suggests that the THz electric field amplitude scales with total sample thickness, d_{tot}.[61] Alternatively, the recent work by Zhang *et al.*,[121] which investigates the thickness dependence of Al (d_{Al} nm)/Co (3 nm) and Pt (d_{Pt} nm)/Co (3 nm) based heterostructures, revealed an optimum layer thickness of 4 nm and an optimum Pt layer thickness of 2-3 nm.[121] These results follow the opposite trend for THz pulse amplitude versus layer thickness which was observed in previous work.[57,60,61] In order to understand the discrepancy between the contrasting results observed by Zhang *et al.*[121] and Wu *et al.*,[61] it is clear that additional material and structural properties, such as interfacial roughness, crystal structure, and strain from the substrate, need to be investigated and their impact further understood.

C. Material properties

Understanding the impact of material properties on the generation of THz radiation produced by spintronic emitters is crucial in order to inform the design of emitters that exhibit optimal performance for commercial, scientific and industrial applications. Whilst the impact of FM/NM material combinations and their thickness dependence upon THz emission have been intensively

researched over recent years, the impact of material properties such as roughness, crystal structure, interfacial intermixing and strain from the substrate have not been widely explored. A systematic study of the emission of THz radiation from Co/Pt bilayers with varying material properties was undertaken by Li *et al.*[124] Here, Co (10 nm)/Pt (3 nm) bilayers were deposited onto glass and Cr-buffered MgO substrates using magnetron sputtering. The table shown in Figure 14 presents results from this study.

The roughness of the Co/Pt interface was varied by changing the Ar sputtering pressure of the Co layer during the deposition. It was shown that decreasing the surface roughness of the Co layer from $\sim$0.2 nm to $\sim$0.1 nm resulted in a smoother Co/Pt interface and an increase in the measured THz electric field strength from 0.8 V cm^{-1} to 2.5 V cm^{-1}, as shown in Figure 14. This factor of $\sim$3 increase in THz electric field amplitude was attributed to a decreasing spin-flip probability at the FM/NM interface with a reduction in the Co/Pt interfacial roughness.[124] Therefore, Li *et al.* report that smoother interfaces become increasingly transparent to spin currents, $\boldsymbol{j}_s$, and suggest that this leads to an increase in the strength of the charge current, $\boldsymbol{j}_c$ generated in the Pt layer via the ISHE.[124] In addition, the effect of varying chemical intermixing at the Co/Pt interface was explored by depositing a 1-2 nm thick Co_xPt_{1-x} alloy spacer layer between the Co and Pt films, where x = 0.25, 0.50 and 0.75. In comparison to the Co/Pt bilayer structure without a spacer layer, the peak THz pulse amplitudes emitted from these heterostructures were up to 4 times greater, where the emission was observed to increase with the level of intermixing, as shown in Figure 14. It has been proposed that the increase in emission of THz radiation in this case could be generated by either: 1) a higher influx of spin currents, due to a reduction of interfacial spin resistivity at the graded Co/Pt interface; or 2) a significant spin-orbit interaction in the Co_xPt_{1-x} spacer layer itself, which could contribute to the spin-to-charge current conversion.[124] Furthermore, the same authors investigated the role of crystal symmetry at the Co/Pt interface using fcc-Co(100)/Pt and hcp-Co(110)/Pt films, grown onto Cr buffered single crystal MgO substrates, as shown in Figure 14. The crystal symmetry at the Co/Pt interface was found to have only a small impact upon the THz electric field amplitude, where effects observed were attributed to the topography related to the crystal interfaces; polycrystalline hcp-Co was reported to form a rougher interface than epitaxial fcc-Co.[124]

In addition to the impact of material properties on the emission of THz radiation, the related effect of post deposition annealing warrants further investigation. This has been studied in CoFeB/W bilayers[67] and also in more complex Ta/CoFeB/MgO/Ta heterostructures,[64] where in general, an-

nealing has been shown to enhance the emission of THz radiation from spintronic emitters.[64,67] Gao *et al.* demonstrated that annealing (post deposition) CoFeB (2.0 nm)/W (2.2 nm) bilayers to a temperature of 280°C, under a uniform external magnetic field of 1 T, led to an increase in peak-to-peak THz electric field amplitude by a factor of 3.[67] This increase in THz emission efficiency was coupled to a decrease in film resistivity, from $\sim$200 $\mu\Omega$ cm (unannealed film) to $\sim$10 $\mu\Omega$ cm (annealed film), and was therefore attributed to an increase in hot electron mean free path as a result of enhanced crystallization with annealing.[67]

The effect of post deposition annealing on the emission of THz radiation from multilayer Ta (5 nm)/CoFeB (t nm)/MgO (2 nm)/Ta (2 nm) heterostructures has been investigated by Sasaki *et al.*,[64] with results from this work shown in Figure 15(a). The authors observed that for heterostructures with a 1 nm thick CoFeB layer, the amplitude of the emitted THz pulse increased by a factor of approximately 1.5 after annealing at a temperature of T_a = 300°C.

Sasaki *et al.* modelled the thickness dependence of the THz emission from Ta/CoFeB/MgO/Ta heterostructures, shown in Figure 15(b), in order to explain the behavior observed experimentally. The model was based upon: 1) the energy density contributed to the system from the pump pulse, 2) impedance matching between the air and the heterostructure, and 3) the attenuation of the spin current in the Ta (heavy metal) layers.[64] Whilst the theoretical transmission intensity of the THz radiation as a function of t_{CFB} predicted a gradual change in the range $t_{CFB} > 1$ nm, the more rapid change which was observed experimentally (except for T_a = 400°C) was attributed to possible backscattering and diffusion of hot electrons, which was not included in the model.[64] It was reported that the significant differences between experimentally observed THz emission dependence on post-deposition annealing (Figure 15(a)) and theoretically predicted behavior (Figure 15(b)) indicates that annealing has a significant effect upon the attenuation of the spin current.[64] The emission dependence on annealing was therefore attributed to the possible spin scattering of electrons with boron atoms, where boron atoms were likely to have diffused into the Ta layer as a consequence of annealing.[64,125] Diffused boron atoms behaving as scattering centers in the adjacent Ta layer could increase the effective spin-Hall angle, α_H, and decrease the hot electron relaxation length, λ_{NM}, thus, increasing the amplitude of the emitted THz radiation.[64] Interestingly, a study by Nenno *et al.*,[126] in which the performance of a Fe (2 nm)/Pt (3 nm) bilayer is modified by defect engineering, demonstrates that the hot electron scattering lifetime, τ_{NM}, can be decreased through increasing the number of defects present in the Pt layer. This result is in agreement with Sasaki *et al.*,[64] as it would lead to a decrease in λ_{NM} and a reduction in the magnitude of the spin current due

to a larger scattering rate.[126] An alternative theory, put forward by Sasaki *et al.*, is that the emission dependence on annealing could be attributed to an increase in velocity and mean free path of hot electrons travelling through an annealed FM CoFeB layer, with a resulting crystalline (001) structure, compared to an unannealed FM CoFeB layer, that exhibits an amorphous structure,[64] which agrees with the study undertaken upon CoFeB/W bilayers by Gao *et al.*[67] This dependence was found to be more significant for thicker films, where, for a post-deposition annealing temperature of $T_a = 400°C$, the THz pulse amplitude for $t_{CFB} = 10\,nm$ increased by a factor of 5 compared to a factor of 2 when $t_{CFB} = 2\,nm$.[64]

Nenno *et al.*[126] report that the differences in the local microstructure of Fe/Pt bilayers can have a dramatic influence on the THz emission. The microstructures of Fe (2 nm)/Pt (3 nm) bilayers grown onto MgO (001) were studied using high resolution zero-loss energy filtered transmission electron microscopy (HR-EFTEM), as shown in Figure 16, for two cases: (a) a sample grown entirely at a deposition temperature of $T_{dep} = 300°C$, and (b) a sample grown at $T_{dep} = 300°C$ for the Fe layer and at room temperature (RT) for the Pt layer.

Comparing the two samples, it was shown that the deformation in the RT-Pt sample was substantially stronger than the Fe/Pt sample grown at $T_{dep} = 300°C$, where deformation was defined by local nm-sized, twisted areas relative to the MgO substrate.[126] Alternatively, depositing the Pt layer at $T_{dep} = 300°C$ led to practically stress-free single crystal growth of Pt.[126] Whilst the relaxation processes of the strained lattices led to local dislocations and vacancies in both samples, it was reported that a higher number of these local defects were present in the RT-Pt sample. The ability of the two samples to emit THz radiation was therefore attributed to the differences in the local microstructure of the Fe/Pt bilayers.[126]

In conclusion, it is clear that material properties such as interfacial roughness, chemical intermixing[124] and post-deposition annealing[64,67] have a significant impact upon the emission of THz radiation from spintronic emitters. The properties of many material systems have yet to be investigated and it is not yet understood how specific materials, thicknesses or substrates effect the generation of THz radiation. Thus, the impact of material properties on the emission process remains a key area of research interest.

D. Ferrimagnetic materials

Whilst numerous studies on spintronic emitters based on ferromagnetic/non-magnetic bilayer material combinations have been reported, the THz emission from ferrimagnetic (FIM)/non-magnetic (NM) bilayers has also been explored. A ferrimagnet, which consists of two magnetically ordered, coupled sublattices, A and B, offers a unique functionality where the different exchange constants J_A and J_B lead to the magnetizations, M_A and M_B having different temperature dependencies.[122] This useful property enables the net magnetization, (M_A + M_B), of the ferrimagnet to be effectively tuned by changing the temperature of the material,[122] where a temperature change can be induced by exposure to femtosecond laser pulses.[62,127,128] FIM/NM THz emitters based upon Gd_xFe_{1-x} alloys have been explored[62,122] as they are archetypal rare-earth transition metal ferrimagnets, exhibiting composition and thickness dependent magnetic properties.[129,130] A recent study by Schneider *et al.*[127] has investigated the composition and magnetic field dependent THz emission from Gd_xFe_{1-x} (20 nm)/Pt (5 nm) heterostructures over the entire composition range ($0 \leq x \leq 1$). Figure 17 reveals how the THz emission varies with applied magnetic field strength. Here, THz pulses with the highest peak-to-peak amplitudes were observed for a maximum applied field of 500 mT.

This observation was attributed to the fully in-plane alignment of the Fe and Gd moments at large applied fields, where H_{app} = 500 mT was shown to saturate the samples with the composition x <0.4.[127] In the case of smaller fields, H_{app} = 50 or 25 mT, which do not fully saturate the samples with a Gd content of x = 0.15 - 0.25, a significant reduction in peak-to-peak THz pulse amplitude[127] was observed during the transition of the magnetic easy axis from an in-plane ($x \leq$ 0.15) to out-of-plane ($x \geq 0.25$) orientation. During this transition, the magnetic compensation point (x = 0.20) appears to have only a small influence on the emitted THz amplitude in comparison to the effect of a spin reorientation. Furthermore, it was found that samples with the composition range of $0.25 \leq x \leq 0.4$, emitted inverted THz pulses which is attributed to the generation of THz radiation at room temperature being dominated by Fe.[127] The authors report that the 800 nm laser-induced spin-polarization of heated electrons in the FIM layer is dominated by the 3d electrons of Fe as they are close to the Fermi energy, whereas the 4f electrons of Gd are 8-11 eV below the Fermi energy and therefore only contribute minimally to the generated THz response.[127] Consequently, the THz waveform flips in polarity when $x \geq 0.25$ since the Fe magnetic moments are aligned antiparallel to the external magnetic field, whereas when $x \leq 0.2$, the

Fe magnetic moments are aligned parallel, inducing the ISHE in opposite directions.[127]

Huisman *et al.*[122] have similarly demonstrated that the emitted THz electric field amplitude from a GdFeCo (20 nm)/Pt (2 nm) heterostructure is dominated by the sensitivity of the FeCo magnetic sublattice to an applied magnetic field, rather than the net magnetization of the GdFeCo layer (M_{FeCo} + M_{Gd}).[122] The dependence of the emitted THz electric field upon applied field, shown in Figure 18, demonstrates that the emission of THz radiation from the heterostructure decreases when the applied field is stronger than 2 T. Similarly to Schneider *et al.*,[127] the THz electric field was observed to undergo a polarity inversion below the compensation temperature of the GdFeCo.[122] This behavior indicates that the THz electric field amplitude is proportional to a linear combination of the in-plane magnetic sublattice components, $aM_{FeCo} + bM_{Gd}$, where $|a| > |b|$ for the polarity inversion to occur.[122] In agreement with Schneider *et al.*, the variation in the sign and the value of a and b was attributed to the fact that the magnetization of the FeCo sublattice occurs from itinerant 3*d* electrons, whilst the magnetization of the Gd sublattice occurs from lower energy level 4*f* electrons, leading to a varying magnetic sublattice sensitivity with respect to the applied magnetic field.[122] Subsequently, Huisman *et al.* demonstrated that this permits the generation of THz radiation from the GdFeCo/Pt bilayer by a spin-polarized current, even when its net magnetization is zero.[122]

This dependency of the THz emission upon net spin polarization, rather than net magnetization, has also been observed by Chen *et al.* in $Co_{1-x}Gd_x$ (7 nm)/Pt (6 nm) heterostructures, where x = 0 - 0.55.[128] At a Gd content of x = 0.26, almost identical to that measured by Schneider *et al.*,[127] the THz pulse was observed to undergo an abrupt polarity inversion without showing a fully quenched signal. This polarity inversion was attributed to the magnetic alignment of the Co sublattice as well as the spin polarization change in direction across the compensation temperature.[128] In addition to the Gd_xFe_{1-x}/Pt bilayers investigated by Schneider *et al.*, a peak THz pulse amplitude was observed in $Co_{1-x}Gd_x$/Pt bilayers when the Gd content was equal to zero.[128] THz pulse amplitudes were observed to decrease with increasing Gd content.[128] This observation, and the thickness dependent properties of $Co_{1-x}Gd_x$, have yet to be fully understood.

More recently, the ability to change the polarity of the THz electric field by tuning the magnetic alignment of sublattices across the compensation temperature[127,128] has been used to control the THz output emission state.[131] In 2020, Fix *et al.*[131] developed a novel Pt/$Gd_{30}Fe_{70}$/W/$Gd_{10}Fe_{90}$/Pt heterostructure in which the varying composition of the two Gd_xFe_{1-x} alloys enabled parallel and antiparallel alignment of their Fe moments with changing temperature above and below the

compensation temperature, T_{comp}, shown in Figure 19. The non-magnetic layers, Pt and W, have opposing spin-Hall angles, which leads to the generation of a large, unidirectional charge current, $\boldsymbol{j}_c$, (see section III.A) when the Fe magnetic moments are aligned antiparallel at a temperature, $T < T_{comp}$. This results in the emission of high-amplitude THz pulses (Figure 19(a)). In comparison, when the Fe magnetic moments are aligned parallel at a temperature, $T > T_{comp}$, the charge current in the two Pt layers flows in opposite directions. Consequently, the THz pulse emitted by the three NM layers combined produces a lower amplitude pulse (Figure 19(b)).[131] These findings demonstrate a potential for ferrimagnetic THz emitter systems which can provide a function for controlled switching of the THz emission from high to low power.[131]

III. IMPACT OF MATERIAL INTERFACES AND INTERFACE ENGINEERING

A. Trilayer and multilayer films

In addition to investigating the choice of thin film materials, research effort has been directed at maximizing the amplitude of the THz radiation pulse emitted from spintronic sources through the study of trilayer[57,58] and multilayer[66] heterostructures. It was first predicted by Seifert *et al.*[57] that the introduction of an additional, second non-magnetic layer (NM_2) layer at the second FM interface of a FM/NM_1 bilayer can boost the amplitude of emitted pulses of THz radiation. In a bilayer structure, only the forward-propagating half of the photoinduced spin current, $\boldsymbol{j}_s$, can flow into the NM_1 layer, where it is converted into a charge current, resulting in a THz pulse being emitted (Figure 2).[57] By introducing the NM_2 layer, it was anticipated that backward-flowing electrons propagating across the resulting NM_2/FM interface can be converted into an additional charge current. Provided that the NM_1 and NM_2 materials exhibit opposite spin-Hall angles, α_H, the charge currents $\boldsymbol{j}_c$ generated in each layer will flow in the same direction, resulting in the emission of a combined THz pulse of increased overall amplitude. Consequently, such a configuration would be expected to increase the efficiency of the spin-to-charge conversion mechanism, and boost the amplitude of the THz radiation emitted.[57] Alternatively, if the spin-Hall angles of the two NM_1 and NM_2 materials are of same sign, then destructive interference will take place due to the induced THz pulses being of opposite polarity. This would result in a reduced overall THz pulse amplitude being observed.

The effect of introducing a second non-magnetic layer was investigated experimentally by

Seifert *et al.*,[57] who observed an increase in the amplitude of the THz pulse emitted from a W (2 nm)/$Co_{40}Fe_{40}B_{20}$ (1.8 nm)/Pt (2 nm) trilayer structure. Comparing the amplitude of the resulting THz pulse to that emitted from a $Co_{40}Fe_{40}B_{20}$/Pt bilayer counterpart structure of equal total thickness, the trilayer produced a THz pulse with a peak amplitude approximately twice that produced by the bilayer structure.[57] This key result has motivated ongoing optimization studies of trilayer spintronic emitters,[58] particularly those which combine W and Pt layers due to their large but opposite values of α_H.[57,58] Peak THz electric fields of 300 KV cm^{-1} have since been measured from W (1.8 nm)/$Co_{20}Fe_{60}B_{20}$ (2.0 nm)/Pt (1.8 nm) trilayers, where the waveforms were observed to exhibit a gapless spectrum, extending from 1 to 10 THz at 10% of its amplitude maximum[58] as shown in Figure 20. Here, the increase in the THz electric field amplitude was achieved by fabricating a large area emitter (7.5 cm diameter). The ability to increase the amplitude of the THz emission by increasing the area of the film offers distinct advantages, in terms of ease of fabrication and use, over traditional emitters such as photoconductor arrays where increased emission is achieved by fabricating arrays of microstructured antenna units[132]. Note that the relatively flat spectral phase observed in Figure 20 indicates that the THz pulse is transform-limited.

In addition to trilayer spintronic emitters, it has been demonstrated that cascaded multilayers can generate strong, broadband THz radiation.[66114] It was theorised by Yang *et al.*[66] that integrating the transverse charge currents generated from several $[NM/FM]_n$ structures can lead to an increase in emission intensity, provided that the transverse charge currents in all NM layers are approximately in-phase. To ensure that $\boldsymbol{j}_c$ was in-phase, structures were produced that consisted of repeating NM/FM layers, separated by thin insulating (I) layers, so that the photoinduced spin current in each FM layer is restricted to flow only into its neighbouring NM layer.[66] Such a design promotes instantaneous excitation at each NM/FM interface in order to achieve in-phase integration of the THz emission.[66] Thus, Yang *et al.* demonstrated experimentally that [Pt (2 nm)/Fe (1 nm)/MgO (2 nm)]$_n$ ($n \geq 1$) cascaded multilayers could enhance the THz electric field strength up to 1.7 times that of a single Fe/Pt bilayer (n = 1), peaking when n = 3 before gradually decreasing as n is increased further, as shown in Figure 21(a).[66]

It was reported that when n >3, the absorption of laser light illuminating the substrate side becomes increasingly significant, leading to a decrease in the number of photoexcited electrons in the top few Fe/Pt bilayers at the film/air interface.[66] The saturation of the THz emission at n = 3, thus, was attributed to this decrease in photoexcited electrons. Nevertheless, Yang *et al.* demonstrated (Figure 21(b)) that the structure with n = 3 repeated layers was, surprisingly, capable

of outperforming a standard 100 μm thick GaP non-linear crystal.[66] Recently, Nenno *et al.*[114] have theoretically investigated the terahertz generation efficiency in cascaded multilayer spintronic systems. In agreement with Yang *et al.*[66], the authors have demonstrated numerically that the current conversion efficiency in an Fe (10nm)/Pt (5 nm) bilayer can be optimized by using n = 3 - 4 repeated bilayers, separated by an insulating layer[114]. However, in contrast to the experimental work by Yang *et al.*[66], the insulating layers in the numerical study were modelled as anti-reflective coatings of thickness $d = 200$ nm, where 200 nm is equivalent to $\frac{\lambda}{4}$ of the incident 800 nm laser pulse. Interestingly, the numerical optimization process revealed a factor of 2 increase in terahertz generation efficiency,[114] which is similar to the experimental results obtained when using 2 nm thick MgO insulating layers.[66]

Subsequently, Feng *et al.*[133] designed a spintronic heterostructure which combined the physical properties of both trilayers[57,58] and cascaded multilayers,[66] to further improve conversion efficiency. The proposed heterostructures consisted of [Pt (1.8 nm)/Fe (1.8 nm)/W (1.8 nm)]$_n$ trilayers (to utilize forward and backward-flowing spin currents), separated by SiO_2 dielectric layers (n = 1,2,3) to promote instantaneous excitation at each pair of NM_1/FM/NM_2 interfaces.[133] In order to tailor absorbance and reflection at multiple layer interfaces,[66] the thickness of the spacer layer was increased from d_{Si} = 2 nm to d_{Si} = 110 nm for n repeated layers. Feng *et al.*[133] observed that the heterostructure with n = 2 and d_{Si} = 110 nm emitted a THz pulse with a peak amplitude $\sim$1.3 times greater than THz pulse emitted from a single heterostructure (n = 1) with the same d_{Si} = 110 nm. Furthermore, for all heterostructures, the amplitude of the THz pulse emitted increased non-linearly with increasing d_{Si}, where this increment was larger with a greater number of repeated layers.[133] This phenomenon, in agreement with predictions of Yang *et al.*,[66] was attributed to the absorption, multiple reflection and interference of THz radiation by the periodic trilayers in each heterostructure. Additionally, Feng *et al.* developed an analytical expression for the emission of THz radiation from the heterostructures, reporting that the emission from a structure with, for example, n = 2 repeating layers is dependent on: (i) the forward-flowing emission from the first NM/FM/NM trilayer which experiences multiple reflections and interference, (ii) the direct forward-flowing emission from the second trilayer and (iii) the backward-flowing emission from the second trilayer which experiences multiple reflections and interference.[133] This was expressed by considering the coefficients of transmission, t_τ, and reflection, r_τ, of THz radiation at

film interfaces,

$$E_{n=2} = \frac{t_\tau e^{ikd}}{1 - r_\tau^2 e^{2ikd}} E_1 + E_2 + \frac{r_\tau t_\tau e^{2ikd}}{1 - r_\tau^2 e^{2ikd}} E_2, \tag{3}$$

where $E_{1,2} = \beta A_{1,2}$ which denotes absorbance, A, of the laser (β is a THz conversion constant), and $2ikd$ denotes the phase accumulation, dependent on the wave vector (k) and SiO_2 thickness (d), during reflection.[133] From this relation, Feng *et al.* demonstrated theoretically and experimentally how the conversion efficiency of $[NM/FM/NM]_n$ cascaded trilayers can be improved by tuning the thickness of the dielectric layer,[133] showing promise for the use of these heterostructures in future THz applications.

B. Rashba-Edelstein effect conversion mechanism

So far, this review has focused upon the emission of helicity independent (HI) pulses of THz radiation from spintronic heterostructures, where the THz pulses are polarized perpendicular to the magnetization of the FM layer.[101] However, in 2013, it was shown by Huisman *et al.*[65] that exciting a spintronic emitter using a circularly polarized fs laser pulse can lead to the emission of an additional helicity dependent (HD) pulse of THz radiation, polarized parallel to the magnetization of the FM layer.[65] In contrast to HI THz pulses, which are generated in the interior of a NM layer by the ISHE spin-to-charge current conversion mechanism,[99,100] it has been shown that HD pulses of THz radiation are generated by an interfacial spin-to-charge current conversion mechanism.[65,67,68,134] This interfacial conversion mechanism is known as the inverse Rashba-Edelstein effect (IREE)[70,135,136] and occurs at interfaces with broken inversion symmetry,[70] such as those between different metals.[65] It has been shown that the IREE is driven by the spin-flip scattering of electrons at these interfaces, known as Rashba interfaces, shown in Figure 22(b).[68] Interfacial Rashba systems have spin-split energy bands, therefore injection of a spin current, $\boldsymbol{j}_s$, into the system leads to an unequal spin accumulation in the two sub-bands.[69] Consequently, the Fermi surface contours are shifted by Δk, shown in Figure 22(a), leading to a non-equilibrium surface density of states.[68] A charge current, $\boldsymbol{j}_c^{IREE}$, carried by the interfacial states, is therefore generated at the Rashba interface, which can be expressed as,[135]

$$\boldsymbol{j}_c^{IREE} = \lambda^{IREE} \cdot \boldsymbol{j}_s = \frac{\alpha_R \, \tau_s}{\hbar} \cdot \boldsymbol{j}_s \tag{4}$$

where α_R is the Rashba coefficient,[136] τ_s is the spin-lattice relaxation time, and λ^{IREE} has the dimension of a length.

Huisman *et al.* excited Co (10 nm)/Pt (2 nm) emitters using circularly polarized laser fs pulses and measured the HD emission, $|E_y|$, polarized parallel to **M** and also the helicity independent (HI) emission, $|E_x|$, polarized perpendicular to **M**, as shown in Figure 23(a). It was found that when the helicity of the fs laser pump was reversed, a change of sign in $|E_y|$ was observed. This demonstrated a dependence of the THz pulse polarization direction, generated by the interfacial IREE conversion mechanism, upon the helicity of the pump pulse,[65] shown in Figure 23(b). In contrast, no change of sign in $|E_x|$ was observed, confirming a helicity independence of the THz electric field polarized perpendicular to **M**. Further fundamental differences between the HD emission and HI emission have been demonstrated, including a contrasting dependence on the thickness of the Pt layer and the amplitude of the THz pulse emitted for the two cases.[65] Huisman *et al.* observed a negligible increase in the HD emission of THz radiation from Co (10 nm)/Pt (d_{Pt}) heterostructures with an increasing thickness of the Pt layer from $d_{Pt} = 2$ nm to 4 nm, which supports the theory that HD THz radiation is being generated at the interface of the heterostructure.[65] In contrast, the HI emission of THz radiation from the same structure was measured to increase from $|E_x| = 25\ \mathrm{V\,cm^{-1}}$ to $100\ \mathrm{V\,cm^{-1}}$ with an increasing thickness of the Pt layer from $d_{Pt} = 2$ nm to 4 nm, which is in agreement with the trend observed for Co/Pt emitters generating pulses of THz radiation by the ISHE conversion mechanism.[61,121] These results highlighted the individual nature of HI and HD THz emission and the differences between the ISHE and IREE spin-to-charge conversion mechanisms for the generation of THz radiation.

Following this work, there has been increased research interest in the use of topological insulators (TI), such as Ag/Bi,[68,69,135] as components of spintronic THz emitters, where FM/NM/TI layered systems have been shown to generate pulses of THz radiation by the IREE.[68,69,135] Initially, spin-pumping experiments were undertaken by Rojas Sánchez *et al.*[135] in order to understand the potential of an IREE spin-to-charge current conversion in NiFe (15 nm)/Ag (d_{Ag} nm)/Bi (8 nm) heterostructures. In their work, conventional ferromagnetic resonance (FMR) and electrical measurement techniques were used to probe the spin dependent properties of the heterostructures, shown in Figure 24. By comparing results obtained from the NiFe/Ag/Bi heterostructure to those measured from NiFe (15 nm)/Ag (5 nm) and NiFe (15 nm)/Bi (8 nm) bilayers, Rojas Sánchez *et al.* reported that the generation of a large spin signal in the NiFe/Ag/Bi heterostructures could only be explained by the occurrence of an IREE at the Ag/Bi interfaces and not by the ISHE of Ag or

Bi.[135] This is because the measured charge current, $\boldsymbol{j}_c^{IREE}$, was observed to decrease to a negligible value with the absence of the Bi layer (Figure 24(a)) which indicated that the contribution from the ISHE in Ag could be neglected.[135] Furthermore a comparatively lower $\boldsymbol{j}_c^{IREE}$ was observed for the NiFe/Bi bilayer (Figure 24(b)), highlighting the necessity of the Ag/Bi interface in generating a large spin signal.

In addition, Rojas Sánchez *et al.* observed that increasing the thickness of the Ag layer from $d_{Ag} = 0$ nm to 10 nm in the NiFe/Ag/Bi heterostructures did not decrease $\boldsymbol{j}_c^{IREE}$. This behavior was attributed to the long spin diffusion length of electrons in Ag, approximately 150 nm at RT,[137] which exceeded the thickness of the Ag layer.[135] In conjunction with the relatively long, ∼50 nm, electron diffusion length in Bi, Rojas Sánchez *et al.* thus reported the spin absorption of Ag and Bi to be negligible (except in their interfacial states). Following this, a simplified relationship between spin current and effective spin mixing conductance was proposed: $\boldsymbol{j}_s \propto G_{\uparrow\downarrow}^{eff}$, where $G_{\uparrow\downarrow}^{eff}$ describes how efficiently spin current can be transmitted from the FM layer to the NM_1/NM_2 interfacial layer states in a $FM/NM_1/NM_2$ heterostructure (taking into account the back flow of electrons).[135]

The observations from Rojas Sánchez *et al.* have generated a growing research interest in spintronic heterostructures with Rashba interfaces for the generation of THz radiation.[68,69] In 2018, the generation of broadband THz radiation was reported, simultaneously, by Jungfleisch *et al.*[68] from a CoFeB/Ag/Bi heterostructure and by Zhou *et al.*[69] from a Fe/Ag/Bi heterostructure, where both samples exhibited the interfacial IREE mechanism. A bandwidth of up to 2.2 THz was exhibited by the CoFeB (2 nm)/Ag (2 nm)/Bi (2 nm) heterostructures (where bandwidth was defined as the frequency at which the intensity drops 10 dB from the maximum),[68] and a bandwidth of up to 4 THz (at 10% of its amplitude maximum) was observed from the Fe/Ag/Bi heterostructures.[69] In agreement with Sánchez *et al.*,[135] Jungfleisch *et al.*[68] showed that increasing the thickness of the Ag layer from $d_{Ag} = 2$ nm to $d_{Ag} = 4$ nm had a negligible effect on the amplitude of the THz radiation emitted. In contrast, when d_{Ag} was increased to 10 nm, the peak THz pulse amplitude was observed to reduce by a factor of 2, however the reasons for this observation are not clear. The relationship between d_{Ag} and the peak THz pulse amplitude has been further explored by Jungfleisch *et al.* using circularly polarized laser pulses.[68] Here, a small HD THz electric field component, $|E_y|$, parallel to the magnetization of the CoFeB layer was observed in CoFeB/Ag/Bi heterostructures, and this dependence was most pronounced when $d_{Ag} = 2$ nm and 4 nm. Interestingly, no helicity dependence was found in the control samples CoFeB/Bi and CoFeB/Pt,[68] which contrasts

to the observation of helicity dependent THz radiation observed from similar Co/Pt structures by Huisman *et al.*[65] Furthermore, Zhou *et al.*[69] confirmed that the emission of HI, broadband THz radiation from Fe/Ag/Bi heterostructures excluded any effects from: (i) demagnetization in the Fe film, (ii) ISHE in bulk Bi or Ag, and (iii) potential signals from other interface states. However, interestingly for these trilayers, when the Bi/Ag interface symmetry was reversed it was found that the THz pulses emitted from Fe (2 nm)/Ag (2 nm)/Bi (3 nm) and Fe (2 nm)/Bi (3 nm)/Ag (2 nm) trilayers were not always 180° out of phase.[69] This result is unusual because a reversal of the interface symmetry, in the case of an ideal Rashba interface, would be expected to reverse the direction of the interfacial electric field, $\hat{\mathbf{z}}$, as shown by equation (5) from Zhou *et al.*,[69]

$$\boldsymbol{j}_c^{IREE} \propto \boldsymbol{\lambda}^{IREE} \boldsymbol{j}_s \times \hat{\mathbf{z}}. \tag{5}$$

Thus, this finding was attributed to the fact that equation (5) is only valid if a perfect Rashba interface exists. Interference effects, including a strong spin orbit coupling, were attributed to the possible surface alloying of AgBi at a thickness of $0 < d_{Bi} < 0.5$ nm, which may have led to a non-negligible spin-Hall effect.[69] Zhou *et al.* subsequently reported a superposition of the measured THz signals by the ISHE and the IREE from heterostructures with a Bi thickness of $0 < d_{Bi} < 0.5$ nm, which could be manipulated by controlling the symmetry of the Ag/Bi interface.[69] This result provided potential for increasing the efficiency of generation of THz radiation from a $FM/NM_1/NM_2$ heterostructure by utilizing the ISHE and IREE in the same device.[69]

Increasing the efficiency of the IREE spin-to-charge current conversion mechanism has recently attracted increasing research interest.[69,134] To date, heterostructures with FM/Ag/Bi Rashba interfaces have achieved peak THz pulse amplitudes up to ∼25% of the amplitudes emitted from FM/NM bilayers,[68] which are favored for their large ISHE efficiency. Additional materials have therefore been investigated for the possibility of increasing the spin-to-charge conversion efficiency and hence $G_{\uparrow\downarrow}^{eff}$. A recent study of the topological insulator Bi_2Se_3, incorporated into the heterostructure $Bi_2Se_3/Co/SiO_2$, revealed temperature independent (from 0 - 300 K) THz emission with a peak electric field amplitude of comparable magnitude to $Pt/Co/SiO_2$ heterostructures.[134]

As shown in Figure 25, the peak THz electric field emission from the Bi_2Se_3/Co heterostructure was measured to be ∼1.7 times that emitted from the Pt(2 nm)/Co (3 nm) heterostructure.[134] This striking result was attributed to the superior spin-to-charge conversion efficiency possessed by spin momentum-locked topological surface states.[134] However this has yet to be fully understood

in order create highly efficient spintronic THz emitters. Overall, it can be seen in Figure 25 that the peak THz electric field emitted from the Pt(6 nm)/Co (3 nm) bilayer still exceeds that of the Bi_2Se_3/Co heterostructure.

C. Introduction of interlayers

To further understand the role of interfaces upon photoinduced current and spin transport, the introduction of interlayers into bilayer or multilayer spintronic THz emitters has been investigated.[138,139] In 2018, Li *et al.*[138] used pulses of circularly polarized laser light to investigate the effect of including Cu and ZnO interlayers (denoted X) in Co (10 nm)/X (d_x nm)/Pt (2.6 nm) heterostructures upon the HD and HI THz emission. In their work, the interlayer thickness, d_x, was increased from 1 nm to 5 nm. It was found that the introduction of a Cu or a ZnO interlayer resulted in a decay in the integrated field strength of both the HD and HI components, $|E_x|$ and $|E_y|$ respectively, as the interlayer thickness was increased, shown in Figure 26.[138] Note that the x and y components of the THz electric field are reversed for Figure 26 in comparison to Figure 23. In the case of the HD components, a gradual exponential decay was observed in $|E_x|$ with increasing thickness of the Cu interlayer (Figure 26(a)), which contrasts with a faster (exponential) decay observed in $|E_x|$ with increasing thickness of ZnO (Figure 26(b)). Furthermore, a complete suppression of the HD component was measured when $d_{ZnO} \geq 2$ nm (Figure 26(b) inset).[138] These results were attributed to the strong dependence of HD THz emission on the quality of the interface between Co and Pt, highlighting the importance of a direct electric contact between the Co and Pt layers for the generation of photoinduced spin current in the helicity dependent case.[138]

Additionally, Li *et al.* report that increasing the thickness of the Cu interlayer leads to a gradual, near linear decay in the HI component, $|E_y|$, (Figure 26(c)). However, increasing the thickness of the ZnO interlayer leads to a strong, exponential decay in the HI component, at a rate $\sim$28 times faster than Cu (Figure 26(d)). This rate was determined by comparing the HI spin diffusion lengths of the Co/ZnO/Pt and Co/Cu/Pt structures, measured to be $l_{ZnO} = 0.4$ nm and $l_{Cu} = 11$ nm). In contrast to the HD THz emission (Figure 26(a,b)), Li *et al.* report that the HI THz emission from Co/X/Pt heterostructures (Figure 26(c,d)) is less sensitive to the interlayer thickness, as $|E_y|$ was observable for $d_x \leq 5$ nm (Figure 26(d) inset) in contrast to the suppression of HD emission when $d_{ZnO} \geq 2$ nm (Figure 26(b) inset).[138]

In contrast to these observations, a recent study by Yang *et al.*[139] indicates that including a Cu

insertion layer in a W/Cu/CoFeB based heterostructure could lead to an enhancement of the emitted HD THz pulse. Using spin-torque FMR and spin-Hall magnetoresistance measurements, the effective spin mixing conductance, $G^{eff}_{\uparrow\downarrow}$, of W (5 nm)/$Co_{40}Fe_{40}B_{20}$ (5 nm)/MgO (2nm)/Ta (2 nm) multilayers were shown to increase by $\sim$25% with the insertion of a 0.52 nm Cu interlayer between the W and CoFeB layers.[139] In addition, an approximately 10% enhancement in interfacial spin transparency, T, was observed with Cu insertion, where T takes into account the effects that lead to electrons being reflected instead of being transmitted at the NM/FM interface.[140] Similarly to Li *et al.*,[138] Yang *et al.* report that both the enhancement of $G^{eff}_{\uparrow\downarrow}$ and T indicate that Cu insertion into W/CoFeB based heterostructures can induce a better interface for the transmission of spin current, and demonstrated, theoretically, that the spin-orbit torque efficiency could be improved by up to 54% using a Cu interlayer of 0.52 nm thickness.[139] Recently, Lu *et al.*[141] have calculated the transmission and reflection of spin current at FM/NM interfaces for a range of material combinations. Using first principle calculations, the authors demonstrate that differences between the reflectivities of spin-up and spin-down electrons at particular FM/NM material interfaces can result in spin filtering, which can be used to improve the spin polarization of the electrons entering the NM layer. The authors report that inserting a thin FM metal or alloy with a high density of states above the Fermi energy, such as Fe, or an anti-reflective coating between the FM and NM layers to act as a 'spin-filter', can lead to an enhancement in the emission of THz radiation due to the increased spin polarization of the hot electrons entering the NM metal,[141] however this has yet to be investigated experimentally. It is clear from these studies[138,139,141] that the impact of introducing interlayers into spintronic heterostructures needs to be further investigated with respect to varying thicknesses, material and spin properties, in order to fully understand their potential for improving the performance of THz emitters.

D. Synthetic antiferromagnetic structures

One of the advantages of spintronic THz emitters is their ability to generate pulses of THz radiation that are polarized perpendicular to the magnetization, **M**, in the plane of the film, and independent to the polarization of the pump laser.[101] This can provide a useful function in allowing the tailoring of the polarization profile of the emitted THz pulse.[102] However, in order to manipulate the polarization profile of the emitted THz pulse, an external magnetic field, H_{app}, is required to define the magnetic state of the FM layer.

However, recently, the emission of THz radiation has been observed from synthetic antiferromagnetic (SAF) structures, without the application of an external field.[142,143] SAF structures consist of two or more exchange-coupled ferromagnetic layers separated by metallic or dielectric spacer layers.[144–146] The interlayer exchange coupling in a SAF structure results from the Ruderman-Kittel-Kasuya-Yosida (RKKY) interaction,[145,146] which is responsible for an oscillatory short-range interaction that can promote ferromagnetic (parallel) alignment or antiferromagnetic (antiparallel) alignment of the FM layers, depending on the spacer layer thickness, d_s.[146,147]

In 2020, Ogasawara *et al.*[142] studied the emission of THz radiation from Ta (3 nm)/CoFeB (2 nm)/Ir (d_s)/CoFeB (2 nm)/Ta (3 nm) synthetic (anti)ferromagnetic structures. The thickness of Ir, d_s, was varied from 0.3 - 1.4 nm to align the magnetization of the two FM layers, $\mathbf{M}_1$ and $\mathbf{M}_2$, antiferromagnetically or ferromagnetically.[142] In the absence of an external field, H_{app}, THz pulses with a maximum electric field amplitude were measured when $\mathbf{M}_1$ and $\mathbf{M}_2$ were aligned antiparallel (d_s = 0.5 nm), as shown in Figure 27. In contrast, increasing d_s to 0.9 nm resulted in the parallel alignment of $\mathbf{M}_1$ and $\mathbf{M}_2$, with the consequence of an almost negligible emitted THz electric field amplitude.[142] This finding was attributed to the variation in structural inversion symmetry between the antiparallel and parallel aligned synthetic (anti)ferromagnetic structure.[142] For parallel alignment of $\mathbf{M}_1$ and $\mathbf{M}_2$, the magnetic and structural inversion symmetry in the synthetic (anti)ferromagnetic structure would, theoretically, lead to the generation of a zero net charge current, $\boldsymbol{j}_c$, due to the positive and negative contributions from the ISHE spin-to-charge conversion mechanism (Figure 27(a)).[142] Consequently, the generation of THz radiation would require an external field to align $\mathbf{M}_1$ and $\mathbf{M}_2$. In contrast, when $\mathbf{M}_1$ and $\mathbf{M}_2$ are aligned in an antiparallel configuration, magnetic inversion symmetry is broken, leading to strong THz emission by the integration of in-phase charge currents in each NM layer of the synthetic antiferromagnetic structure.[142] Ogasawara *et al.* subsequently demonstrated that applying an external field to the parallel aligned synthetic (anti)ferromagnetic structure, in order to break the magnetic inversion symmetry, leads to a small increase in the electric field amplitude of the THz pulses. Applying the same magnetic field to the antiparallel configuration resulted in a significant decrease in the THz electric field amplitude, as shown in Figure 27(b).[142] These results indicate a strong dependence of THz emission upon antiferromagnetic interlayer coupling, and demonstrate the potential of SAF structures for field-free generation of THz radiation.

Also in 2020, Zhang *et al.*[143] reported the emission of THz radiation from Fe-Mn-Pt based SAF structures. However, this was achieved using a different mechanism to that proposed by Ogasawara

et al. Until very recently, only two current conversion mechanisms for the generation of THz radiation from a spintronic source have been widely studied - the inverse spin-Hall effect[99,100] and the inverse Rashba-Edelstein effect.[70,135,136] However, in 2019, Zhang *et al.* demonstrated that THz radiation could be generated from a single layer ferromagnet by an additional mechanism known as the anomalous spin-Hall effect (AHE).[148] The AHE, shown in Figure 28, acts as a mechanism for generating spin current in conducting ferromagnets with broken time-reversal symmetry.[149] When a current, I, flows into a FM layer in a longitudinal direction, spin-up ($\uparrow$) and spin-down ($\downarrow$) electrons are deflected to traverse in opposite directions through the FM layer.[149] This process is thought to occur due to underlying extrinsic mechanisms such as skew scattering[150] and side jump,[151] or intrinsic mechanisms which relate to the band structure of the material.[152] In the FM layer, the asymmetry in density of states at the Fermi level gives rise to transverse charge current, $\boldsymbol{j}_c$, and spin accumulation of electrons at the boundaries of the ferromagnet (Figure 28).[149] This leads to the generation of an anomalous Hall voltage, V_H, across the FM layer, simultaneously with a spin current, $\boldsymbol{j}_s$, perpendicular to the magnetization $\mathbf{M}$.[149]

The AHE conversion mechanism was initially utilized by Zhang *et al.*[148] to generate pulses of THz radiation from a single layer ferromagnet. In their study, a fully saturated $(Fe_{80}Mn_{20})_{67}Pt_{33}$ (3 nm) ferromagnet, capped with dielectric MgO (4 nm), was irradiated using a femtosecond laser with a fluence of 0.55 mJ cm^{-2}. Following excitation, non-thermal, superdiffusive electrons were reflected at the substrate/ferromagnet and the ferromagnet/dielectric interfaces, which induced a backflow of current through the ferromagnet.[148] The amplitude and polarity of the backflow current was attributed to the material properties and roughness of the interfaces, where the smoother (substrate/ferromagnet) interface produced a larger backflow current than the rougher (ferromagnet/dielectric) interface in the structure.[148] This led to the formation of a net longitudinal current, $\boldsymbol{I}_N$, in the FM layer which, with the presence of the AHE, was converted to a transient, transverse current,[148]

$$\boldsymbol{j}_c = \alpha_{AHE}\mathbf{M} \times \boldsymbol{I}_N, \tag{6}$$

where α_{AHE} is the AHE angle. This resulted in the emission of pulses of THz radiation, dependent on: 1) the direction of the applied magnetic field, where positive H_{app} led to the emission of positive E_{THz}; 2) the strength of the AHE in the FM layer, where greater THz pulse amplitudes were measured from $(Fe_{80}Mn_{20})_{67}Pt_{33}$ and $Ni_{80}Fe_{20}$ with larger AHE than $Fe_{80}Mn_{20}$ and $Co_{20}Fe_{60}B_{20}$, and 3) the thickness of the FM layer, where peak THz pulse amplitudes were observed when d_{FM}

= 3-4 nm in $(Fe_{80}Mn_{20})_{67}Pt_{33}$ films.[148]

Zhang *et al.* reported the emission of THz radiation from $(Fe_{80}Mn_{20})_{67}Pt_{33}$ (4 nm)/Ru (0.8 nm)/ $(Fe_{80}Mn_{20})_{67}Pt_{33}$ (4 nm)/MgO (4 nm) SAF structures, by the AHE mechanism,[143] where peak THz pulse amplitudes were almost double that of corresponding single layer emitters of the equivalent thickness.[143] In these SAF structures, the thickness of the Ru layer, d_s, promotes antiparallel alignment of the magnetization of two FM layers, $\mathbf{M}_1$ and $\mathbf{M}_2$, as shown in Figure 29(a). Therefore, when irradiated by fs laser pulses, in the absence of an applied field, nonthermal, superdiffusive spin currents which were reflected from the substrate/ferromagnet and the ferromagnet/dielectric interfaces flow in opposite directions through each FM layer in the SAF structure. Subsequently, due to the opposite polarity of $\mathbf{M}_1$ and $\mathbf{M}_2$, shown in Figure 29(a), both longitudinal currents flowing in each FM layer were converted into transverse charge currents with the same polarity via the AHE, with a net, transverse charge-current density $\boldsymbol{j}_c \propto (\mathbf{M}_1 + \mathbf{M}_2)$ x $\hat{\mathbf{z}}$, where $\hat{\mathbf{z}}$ is a unit vector along the z axis (Figure 29(a)).[143] This was reported to lead to the emission of THz radiation from the antiparallel aligned SAF structure when $H_{app} = 0$, shown in Figure 29(b), which was attributed to the constructive contribution of the charge currents generated in each FM layer.[143]

In comparison, the application of an external field H = 200 Oe, which was strong enough to saturate the SAF structure so that $\mathbf{M}_1$ and $\mathbf{M}_2$ aligned in parallel, was found to reduce the electric field amplitude of the THz pulse emitted from the structure by ~30%. As shown in Figure 29(b), the electric field amplitude emitted from the parallel aligned SAF structure is proportional to the response measured from the original 5 nm thick single layer Fe-Mn-Pt ferromagnet.[148] By treating the parallel aligned SAF structure as a single layer emitter with an equivalent thickness of 8.8 nm, Zhang *et al.* demonstrate consistency between the results from the two studies which demonstrate an AHE driven emission of THz radiation.[143,148]

More significantly, Zhang *et al.* demonstrated that incorporating a single layer ferromagnet[148] into an antiparallel aligned SAF structure will not only enhance the AHE driven THz emission, but will also provide field-free THz emission from a spintronic heterostructure at room temperature.[143] In conjunction with the observation of field-free THz emission from a SAF structure by Ogasawara *et al.*,[142] it is clear that these novel structures could have great potential for use in a large range of THz applications.

IV. DISCUSSION AND OUTLOOK

Since the discovery in 2013[101] that novel thin film ferromagnetic (FM)/non-magnetic (NM) bilayers can be utilized to generate THz radiation, researchers have focused on investigating how different thin film materials affect the emission. A key goal has been to create structures that improve the emission amplitude of the THz pulse produced. In less than a decade, researchers have developed a coherent understanding of how the ISHE spin-to-charge current conversion mechanism results in the generation of sub-picosecond, linearly polarized pulses of THz radiation from such emitters.[99,100] Furthermore, a range of material, structural and interfacial properties have been investigated, as well as the use of trilayer and multilayer structures, in order to understand what is required to optimize the performance of spintronic THz emitters.

Following the realization that the choice of NM material could greatly enhance the electric field amplitude and bandwidth of the pulse of THz radiation emitted from a FM/NM bilayer,[101] the impact of different FM/NM material combinations on emission, and their thickness dependence, has been studied in detail.[57,60–62,121] Whilst the choice of FM material does not appear to have a significant impact on emission (with the exception of Ni due to its low Curie temperature, 627 K),[57,60] it is now well established that peak THz electric field amplitudes can be achieved by using NM materials with a high electron mobility and a large spin-Hall conductivity[60,101] such as Pt.[57,58,61,62,65,124] These findings have led to a large research focus on CoFeB/Pt,[57,58,133] Co/Pt,[62,65,124,138] and Fe/Pt[66,126] based heterostructures as high performing THz emitters. Furthermore, thickness dependence studies on a range of FM/NM material combinations, including CoFeB/Pt,[57] CoFeB/Pd,[60] Co/Pt,[61,121] and Co/W[57,61] have reported that peak THz pulse amplitudes and bandwidths are emitted when the FM layers and NM layers are 1-3 nm thick.[57,60,61,121] Note that the electric field amplitudes reported in these studies are difficult to compare directly due to the different characteristics of the individual measurement systems and the lack of coherency in the units used. As the development of spintronic emitters continues, there needs to be a move away from comparative measurements of the amplitude of THz waveforms, often presented in arbitrary units, to measurements that enable the merits of emitters developed by different groups to be directly compared. While there is no single figure-of-merit to characterize the performance of a terahertz emitter, as the important parameter often depends on the application, the measured peak electric field focused at the detector, the measured terahertz pulse energy, and the calculated optical-to-terahertz conversion efficiency are all widely used in comparing the performance

of nonlinear crystals and photoconductive antennas[153] and should be employed. This information together with experimental details on the THz emitter area, the pump excitation fluence, and the collection and focusing optics employed, can allow for quantitative comparisons between spintronic emitter designs. We note that the terahertz pulse energy and peak electric field emitted from a spintronic emitter has been measured by Seifert et al.,[58] where a THz pulse energy of 5.1 nJ and electric field of 300 kV cm^{-1} was obtained by photoexcitaton of a large-area (7.5 cm diameter) trilayer structure using a 40 fs pulse with a central wavelength of 800 nm and a pulse energy of 5.5 mJ. Work reporting this level of detail is uncommon but will be essential in the future if progress is to be made.

Studies have shown that the magnitude and polarity of the emitted THz pulse correlates with the amplitude and sign of the spin-Hall angle of the NM material chosen.[57,61] This useful electrical property has been exploited to improve the ISHE spin-to-charge current conversion mechanism in the heterostructures by the development of NM_1/FM/NM_2 trilayer emitters, where NM_1 and NM_2 have large but opposing spin-Hall angles (such as W and Pt).[57,58,133] Peak THz pulse amplitudes, approximately twice those for bilayer structures, have been observed from trilayer spintronic emitters of equal total thickness.[57] This has motivated the ongoing study of trilayers[58] and cascaded trilayers, $[NM_1/FM/NM_2]_n$,[114,133] for improving the amplitude of spintronic emitters. It is possible that with effective optimization of the appropriate material properties and layer thicknesses,[114,133] these novel structures will have significant potential for use in a wide range of THz applications.

Whilst the impact of different FM/NM material combinations on the THz emission have been well documented for some thin film structures, the effects of material properties such as roughness, crystal structure, interfacial intermixing and strain from the substrate on emission have not been widely reported. Ongoing studies have, so far, demonstrated that these properties can have a critical impact upon the generation of THz radiation from particular systems including Co/Pt,[124] Ta/CoFeB,[64] and CoFeB/W based heterostructures[67]. In particular, it was shown by Li *et al.*[124] that a reduction in the roughness of the interface, as well as increased chemical intermixing at the interface can lead to up to a factor of 2 improvement in the THz pulse amplitude in a Co/Pt heterostructure, due to a possible reduction of interfacial spin resistivity.[124] Furthermore, post-deposition annealing has been observed to significantly increase the intensity of the THz radiation emitted from heterostructures containing CoFeB.[64,67] The enhancement of the THz pulse amplitude with annealing has been attributed to either: the diffusion of B atoms into the NM layer, leading to increased spin scattering and increased effective spin-Hall angle, α_H,[64,126] or the relax-

ation of strained lattices, leading to an increase in mean free path of hot electrons.[64,67,126] It is clear that further studies need to be undertaken to fully understand the significance of each mechanism and that a wider range of thin film heterostructures need to be explored to fully understand their influence on spin transport and the generation of THz radiation.

Whilst the majority of research for high performing THz emitters has largely focused upon Pt based heterostructures,[57,58,62,65,66,124,126,133,138] recently, light metals such as Al[121] have been revisited as potential, cost-effective, alternative NM films in spintronic emitters. Despite the large difference between the spin-Hall angle of Al (0.03%) and Pt (3%), the maximum THz electric field amplitude of Al/Co bilayers was still observed to be significant, approximately 34% of that found in Pt/Co bilayers.[121] The physical origin of this result is not clear,[121] highlighting the need for further experiments on these potentially cost-effective systems. Other systems investigated for application in room temperature spintronic THz emitters include ferrimagnetic (FIM)/NM bilayers, where optimization has focused largely upon tailoring the composition and thickness of the FIM layer.[62,122,127,128] The realization of a polarity inversion in the THz electric field below the compensation temperature of Gd_xFe_{1-x}/Pt,[122] Gd_xCo_{1-x}/Pt,[128] and GdFeCo/Pt[127] bilayers offers great potential for output control of spintronic THz emitting systems. Subsequently, a novel NM/Gd_xFe_{1-x}/NM/Gd_xFe_{1-x}/NM heterostructure has been proposed that demonstrates the ability to control the emitting state (high- or low-amplitude) of the THz radiation, depending on the relative alignment of the Fe moments.[131]

Whilst the use of FIM materials offer the ability to control the polarity of the emitted THz radiation from a spintronic heterostructure, it has been shown that the polarization profile of THz pulses can also be manipulated by the shape of the applied magnetic field.[102] The ability to produce polarization profiles with radial components could offer high efficiency coupling of THz radiation to cylindrical wire waveguides,[120] and such profiles could also provide enhanced longitudinal electric field components when focused,[102] which has applications in particle acceleration.[154] Furthermore, the THz electric field emitted from a spintronic heterostructure can be manipulated by the helicity of light, which may provide opportunities for wireless spintronics applications.[68] The polarity of the HD THz emission from a Co/Pt bilayer has been shown to invert when the helicity of light is reversed,[65] which has been attributed to the generation of THz radiation by the interfacial IREE spin-to-charge current conversion mechanism.[65,68,69] Discovery of the IREE conversion mechanism in structures with broken symmetry interfaces[70,135,136] has stimulated a research drive to understand the influence of the interfacial properties upon the generation of THz

radiation. Here, initial studies using FM/Ag/Bi trilayers with Rashba interfaces,[68,69] have led to the significant measurement of a superimposed THz signal, generated by the ISHE and IREE simultaneously.[69] This demonstrates a potential to create spintronic THz emitters with increased electric field amplitudes by utilizing both spin-to-charge current conversion mechanisms in the same device. However, this has yet to be explored experimentally. Following the reports of highly efficient IREE spin-to-charge current conversion in Bi_2Se3/Co based heterostructures,[134] it is clear that additional materials need to be considered in order to understand the role of interfaces upon the generation of THz radiation.

Field-free emission of THz radiation has been observed from SAF structures at room temperature by both the ISHE and the AHE mechanisms.[143] This key development highlights the potential of spintronic emitters based on SAF structures for applications requiring tunable polarization.[143] The possibility to generate THz radiation without an external field makes such emitters easier to construct and use. Furthermore, it has been shown that the AHE mechanism, similarly to the ISHE, leads to a dependency of the emitted THz pulse amplitude on the thickness of the FM layer.[148] However, the AHE conversion mechanism has yet to explored in more than a small number of heterostructures.[143,148]

In summary, spintronic THz emitters have already demonstrated several desirable source characteristics, including a gapless broadband emission reaching up to 30 THz, the requirement for only nano-joule energy pulses,[57] scalability for the generation of high THz field amplitudes (up to $300\,\mathrm{kV\,cm^{-1}}$),[58] and appear to be independent of the photo-excitation wavelength.[59]

It is evident that there are still a multitude of avenues to investigate in order to optimize spintronic heterostructures to create idealized emitters that can generate high amplitude, broadband pulses of THz radiation. Promising areas of investigation that have been highlighted from the research presented in this review include:

1) The optimization of material properties, such as tailoring the microstructure, strain or defect engineering in trilayer or multilayer heterostructures. This has demonstrated a potential for the improvement of spin-to-charge conversion efficiency. However, it is also important to consider strategic materials to use in these systems, where further study into the material properties of light metal/FM based heterostructures potentially offer significant advantage.

2) Interface engineering of FM/NM (heavy metal) and FM/NM/NM Rashba systems in order to fully understand the role of interfaces upon the generation of THz radiation in a variety of materials. An increased understanding of interfacial phenomena could allow for simultaneous utilization

of the ISHE and IREE conversion mechanisms in the same structure, ultimately leading to THz emitters with an increased emission amplitude.[69]

3) The continued development of recently proposed THz emitters based upon synthetic antiferromagnetic structures for the field-free generation of THz radiation at room temperature. Exploring the geometry of emitters based upon SAF structures could enable the future development of easy to construct THz emitters with tuneable polarizations.[143]

4) The further investigation of thin film materials which exhibit a very large anomalous Hall effect for the generation of THz radiation utilising the AHE conversion mechanism.[143] This category of materials includes magnetic Weyl semi-metals, which are the subject of significant current research activity, where the anomalous Hall angle is reported to be an order of magnitude greater than typically found in magnetic systems.[155,156] Recent theoretical work has also predicted that it may be possible to generate spin currents whose polarization can be in any direction.[157] If this could be realized experimentally, then it may be possible to create homogeneous structures that trigger even greater emission amplitudes.

Given the relatively low cost of spintronic THz emitters (in comparison to PCAs and nonlinear crystals) and their already competitive source parameters, together with the potential for further significant development, means they are extremely promising sources for THz time-domain spectroscopy and its exploitation in scientific research and industrial applications.

ACKNOWLEDGMENTS

This work was supported by the United Kingdom Engineering and Physical Sciences Research Council [Grant No. EP/S033688/1]. We also wish to acknowledge the PhD scholarship support for R. Ji by the China Scholarship Council (NSCIS No. 201906120039).

DATA AVAILABILITY

Data sharing is not applicable to this article as no new data were created or analyzed in this study.

REFERENCES

[1]D. H. Auston, K. P. Cheung, and P. R. Smith, "Picosecond photoconducting Hertzian dipoles," Appl. Phys. Lett. **45**, 284 (1984).

[2]D. H. Auston, *Picosecond Optoelectronic Devices* (New York:Academic, 1987).

[3]J. A. Spies, J. Neu, U. T. Tayvah, M. D. Capobianco, B. Pattengale, S. Ostresh, and C. A. Schmuttenmaer, "Terahertz spectroscopy of emerging materials," J. Phys. Chem. C **124**, 22335 (2020).

[4]P. D. Cunningham, N. N. Valdes, F. A. Vallejo, L. M. Hayden, B. Polishak, X.-H. Zhou, J. Luo, A. K.-Y. Jen, J. C. Williams, and R. J. Twieg, "Broadband Terahertz characterization of the refractive index and absorption of some important polymeric and organic electro-optic materials," J. Appl. Phys. **109**, 043505 (2011).

[5]M. T. Hibberd, V. Frey, B. F. Spencer, P. W. Mitchell, P. Dawson, M. J. Kappers, R. A. Oliver, C. J. Humphreys, and D. M. Graham, "Dielectric response of Wurtzite Gallium Nitride in the Terahertz frequency range," Solid State Commun. **247**, 68 (2016).

[6]D. Alves-Lima, J. Song, A. P. X. Li, Y. Shen, J. A. Zeitler, and H. Lin, "Review of Terahertz pulsed imaging for pharmaceutical film coating analysis," Sensors **20**, 1441 (2020).

[7]K. Su, Y.-C. Shen, and J. A. Zeitler, "Terahertz sensor for non-contact thickness and quality measurement of automobile paints of varying complexity," IEEE Trans. Terahertz Sci. Technol. **4**, 432 (2014).

[8]M. Naftaly, N. Vieweg, and A. Deninger, "Industrial applications of Terahertz sensing: State of play," Sensors **19**, 4203 (2019).

[9]L. Yang, T. Guo, X. Zhang, S. Cao, and X. Ding, "Toxic chemical compound detection by Terahertz spectroscopy: a review," Rev. Anal. Chem. **37**, 20170021 (2018).

[10]H. Zhong, A. Redo-Sanchez, and X.-C. Zhang, "Identification and classification of chemicals using Terahertz reflective spectroscopic focal-plane imaging system," Opt. Express **14**, 9130 (2006).

[11]V. A. Trofimov and S. A. Varentsova, "A possible way for the detection and identification of dangerous substances in ternary mixtures using THz pulsed spectroscopy," Sensors **19**, 2365 (2019).

[12]M. Awad, M. Nagel, H. Kurz, J. Herfort, and K. Ploog, "Characterization of low temperature GaAs antenna array Terahertz emitters," Appl. Phys. Lett. **91**, 181124 (2007).

[13]A. Dreyhaupt, S. Winnerl, T. Dekorsy, and M. Helm, "High-intensity Terahertz radiation from a microstructured large-area photoconductor," Appl. Phys. Lett. **86**, 121114 (2005).

[14]C. W. Berry, N. Wang, M. R. Hashemi, M. Unlu, and M. Jarrahi, "Significant performance enhancement in photoconductive Terahertz optoelectronics by incorporating plasmonic contact electrodes," Nat. Commun. **4**, 1622 (2013).

[15]P. J. Hale, J. Madeo, C. Chin, S. S. Dhillon, J. Mangeney, J. Tignon, and K. M. Dani, "20 THz broadband generation using semi-insulating, GaAs interdigitated photoconductive antennas," Opt. Express **22**, 26358 (2014).

[16]Y. C. Shen, P. C. Upadhya, E. H. Linfield, and H. E. Beere, "Ultrabroadband Terahertz radiation from low-temperature-grown GaAs photoconductive emitters," Appl. Phys. Lett. **83**, 3117 (2003).

[17]D. R. Bacon, T. B. Gill, M. Rosamond, A. D. Burnett, A. Dunn, L. Li, E. H. Linfield, A. G. Davies, P. Dean, and J. R. Freeman, "Photoconductive arrays on insulating substrates for high-field Terahertz generation," Opt. Express **28**, 17219 (2020).

[18]M. Beck, H. Schäfer, G. Klatt, J. Demsar, S. Winnerl, M. Helm, and T. Dekorsy, "Impulsive Terahertz radiation with high electric fields from an amplifier-driven large-area photoconductive antenna," Opt. Express **18**, 9251 (2010).

[19]D. You, R. R. Jones, P. H. Bucksbaum, and D. R. Dykaar, "Generation of high-power sub-single-cycle 500-fs electromagnetic pulses," Opt. Lett. **18**, 290 (1993).

[20]E. Budiarto, J. Margolies, S. Jeong, J. Son, and J. Bokor, "High-intensity Terahertz pulses at 1-kHz repetition rate," IEEE J. Quantum Electron. **32**, 1839 (1996).

[21]T. Hattori, K. Tukamoto, and H. Nakatsuka, "Time-resolved study of intense Terahertz pulses generated by a large-aperture photoconductive antenna," Jpn. J. Appl. Phys. **40**, 4907 (2001).

[22]K. Kuznetsov, A. Klochkov, A. Leontyev, E. Klimov, S. Pushkarev, G. Galiev, and G. Kitaeva, "Improved InGaAs and InGaAs/InAlAs photoconductive antennas based on (111)-oriented substrates," Electronics **9**, 495 (2020).

[23]I. Kostakis, D. Saeedkia, and M. Missous, "Terahertz generation and detection using low temperature grown InGaAs-InAlAs photoconductive antennas at 1.55 μm pulse excitation," IEEE Trans. Terahertz Sci. Technol. **2**, 617 (2012).

[24]A. Takazato, M. Kamakura, T. Matsui, J. Kitagawa, and Y. Kadoya, "Terahertz wave emission and detection using photoconductive antennas made on low-temperature-grown InGaAs with 1.56 μm pulse excitation," Appl. Phys.Lett. **91**, 011102 (2007).

[25]A. Nahata, A. S. Weling, and T. F. Heinz, "A wideband coherent terahertz spectroscopy system using optical rectification and electro-optic sampling," Appl. Phys. Lett. **69**, 2321 (1996).

[26]Q. Guoa, Y. Kumea, Y. Fukuharaa, T. Tanakaa, M. Nishioa, H. Ogawaa, M. Hiratsukab, M. Tanib, and M. Hangyob, "Observation of ultra-broadband terahertz emission from ZnTe films grown by metaloganic vapor epitaxy," Solid State Commun. **141**, 188 (2007).

[27]P. Y. Han and X.-C. Zhang, "Free-space coherent broadband Terahertz time domain spectroscopy," Meas. Sci. Technol. **12**, 1747 (2001).

[28]G. L. Dakovski, B. Kubera, and J. Shan, "Localized terahertz generation via optical rectification in ZnTe," J. Opt. Soc. Am. **22**, 1667 (2005).

[29]F. Blanchard, L. Razzari, H.-C. Bandulet, G. Sharma, R. Morandotti, J.-C. Kieffer, T. Ozaki, M. Reid, H. F. Tiedje, H. K. Haugen, and F. A. Hegmann, "Generation of 1.5 μj single-cycle terahertz pulses by optical rectification from a large aperture ZnTe crystal," Opt. Express **15**, 13212 (2007).

[30]S. Vidal, J. Degert, M. Tondusson, J. Oberlé, and E. Freysz, "Impact of dispersion, free carriers, and two-photon absorption on the generation of intense Terahertz pulses in ZnTe crystals," App. Phys. Lett. **98**, 191103 (2011).

[31]T. Löffler, T. Hahn, M. Thomson, F. Jacob, and H. G. Roskos, "Large-area electro-optic ZnTe Terahertz emitters," Opt. Express **13**, 5353 (2005).

[32]S. M. Harrel, R. L. Milot, J. M. Schleicher, and C. A. Schmuttenmaer, "Influence of free-carrier absorption on Terahertz generation from ZnTe (110)," J. Appl. Phys. **107**, 033526 (2010).

[33]K. Aoki, J. Savolainen, and M. Havenith, "Broadband Terahertz pulse generation by optical rectification in GaP crystals," Appl. Phys. Lett. **110**, 201103 (2017).

[34]G. Chang, C. J. Divin, C.-H. Liu, S. L. Williamson, A. Galvanauskas, and T. B. Norris, "Power scalable compact THz system based on an ultrafast Yb-doped fiber amplifier," Opt. Express **14**, 7909 (2006).

[35]J. Drs, N. Modsching, C. Paradis, C. Kränkel, V. J. Wittwer, O. Razskazovskaya, and T. Südmeyer, "Optical rectification of ultrafast Yb lasers: pushing power and bandwidth of terahertz generation in GaP," J. Opt. Soc. Am. B **36**, 3039 (2019).

[36]H. Hirori, A. Doi, F. Blanchard, and K. Tanaka, "Single-cycle Terahertz pulses with amplitudes exceeding 1 MV/cm generated by optical rectification in $LiNbO_3$," Appl. Phys. Lett. **98**, 091106 (2011).

[37]X.-J. Wu, J.-L. Ma, B.-L. Zhang, S.-S. Hai, Z.-J. Fang, C.-Y. Xia, D.-Y. Kong, J.-G. Wang, H. Liu, C.-Q. Zhu, X. Wang, C.-J. Ruan, and Y.-T. Li, "Highly efficient generation of 0.2 mj terahertz pulses in lithium niobate at room temperature with sub-50 fs chirped Ti:sapphire laser pulses," Opt. Express **26**, 7107 (2018).

[38]P. Y. Han, M. Tani, F. Pan, and X.-C. Zhang, "Use of the organic crystal DAST for Terahertz beam applications," Opt. Lett. **25**, 675 (2000).

[39]C. Vicario, M. Jazbinsek, A. V. Ovchinnikov, O. V. Chefonov, S. I. Ashitkov, M. B. Agranat, and C. P. Hauri, "High efficiency THz generation in DSTMS, DAST and OH1 pumped by Cr:forsterite laser," Opt. Express **23**, 4573 (2015).

[40]C. Somma, G. Folpini, J. Gupta, K. Reimann, M. Woerner, and T. Elsaesser, "Ultra-broadband Terahertz pulses generated in the organic crystal DSTMS," Opt. Lett. **40**, 3404 (2015).

[41]M. Shalaby and C. P. Hauri, "Demonstration of a low-frequency three-dimensional terahertz bullet with extreme brightness," Nat. Commun. **6**, 5976 (2015).

[42]Y. Zhang, X. Zhang, S. Li, J. Gu, Y. Li, Z. Tian, C. Ouyang, M. He, J. Han, and W. Zhang, "A Broadband THz-TDS System Based on DSTMS Emitter and LTG InGaAs/InAlAs Photoconductive Antenna Detector," Sci. Rep. **6**, 26949 (2016).

[43]A. G. Stepanov, C. Ruchert, J. Levallois, C. Erny, and C. P. Hauri, "Generation of broadband THz pulses in organic crystal OH1 at room temperature and 10 K," Opt. Mater. Express **4**, 870 (2014).

[44]H. Zhao, Y. Tan, T. Wu, G. Steinfeld, Y. Zhang, C. Zhang, L. Zhang, and M. Shalaby, "Efficient broadband Terahertz generation from organic crystal BNA using near infrared pump," Appl. Phys. Lett. **114**, 241101 (2019).

[45]H. G. Roskos, M. D. Thomson, M. Kreß, and T. Löffler, "Broadband THz emission from gas plasmas induced by femtosecond optical pulses: From fundamentals to applications," Laser Photonics Rev. **1**, 349 (2007).

[46]B. Clough, J. Dai, and X.-C. Zhang, "Laser air photonics: Beyond the Terahertz gap," Mater. Today **15**, 50 (2012).

[47]T. Bartel, P. Gaal, K. Reimann, M. Woerner, and T. Elsaesser, "Generation of single-cycle THz transients with high electric-field amplitudes," Opt. Lett. **30**, 2805 (2005).

[48]M. D. Thomson, V. Blank, and H. G. Roskos, "Terahertz white-light pulses from an air plasma photo-induced by incommensurate two-color optical fields," Opt. Express **18**, 23173 (2010).

[49]E. Matsubara, M. Nagai, and M. Ashida, "Ultrabroadband coherent electric field from far infrared to 200 THz using air plasma induced by 10 fs pulses," Appl. Phys. Lett. **101**, 011105 (2012).

[50]I. Dey, K. Jana, V. Y. Fedorov, A. D. Koulouklidis, A. Mondal, M. Shaikh, D. Sarkar, A. D. Lad, S. Tzortzakis, A. Couairon, and G. R. Kumar, "Highly efficient broadband Terahertz generation from ultrashort laser filamentation in liquids," Nat. Commun. **8**, 1184 (2017).

[51]L. Luo, I. Chatzakis, J. Wang, F. B. P. Niesler, M. Wegener, T. Koschny, and C. M. Soukoulis, "Broadband Terahertz generation from metamaterials," Nat. Commun. **5**, 3055 (2014).

[52]N. M. Burforda and M. O. El-Shenawee, "Review of Terahertz photoconductive antenna technology," Opt. Eng. **56**, 010901 (2017).

[53]E. Isgandarov, X. Ropagnol, M. Singh, and T. Ozaki, "Intense terahertz generation from photoconductive antennas," Front. Optoelectron. (2020), 10.1007/s12200-020-1081-4.

[54]A. Singh, A. Pashkin, S. Winnerl, M. Welsch, C. Beckh, P. Sulzer, A. Leitenstorfer, M. Helm, and H. Schneider, "Up to 70 THz bandwidth from an implanted Ge photoconductive antenna excited by a femtosecond Er:fibre laser," Light Sci. Appl. **9**, 30 (2020).

[55]M. Jazbinsek, U. Puc, A. Abina, and A. Zidansek, "Organic Crystals for THz Photonics," Appl. Sci. **9**, 882 (2019).

[56]J. A. Fülöp, S. Tzortzakis, and T. Kampfrath, "Laser-Driven Strong-Field Terahertz Sources," Adv. Optical Mater. **8**, 1900681 (2020).

[57]T. Seifert, S. Jaiswal, U. Martens, J. Hannegan, L. Braun, P. Maldonado, F. Freimuth, A. Kronenberg, J. Henrizi, I. Radu, E. Beaurepaire, Y. Mokrousov, P. M. Oppeneer, M. Jourdan, G. Jakob, D. Turchinovich, L. M. Hayden, M. M. Wolf, M. Münzenberg, K. . T, and Kampfrath, "Efficient metallic spintronic emitters of ultrabroadband Terahertz radiation," Nat. Photonics **10**, 483 (2016).

[58]T. Seifert, S. Jaiswal, M. Sajadi, G. Jakob, S. Winnerl, M. Wolf, M. Kläui, , and T. Kampfrath, "Ultrabroadband single-cycle Terahertz pulses with peak fields of 300 kV cm-1 from a metallic spintronic emitter," Appl. Phys. Lett. **110**, 252402 (2017).

[59]R. I. Herapath, S. M. Hornett, T. S. Seifert, G. Jakob, M. Kläui, J. Bertolotti, T. Kampfrath, and E. Hendry, "Impact of pump wavelength on Terahertz emission of a cavity-enhanced spintronic trilayer," Appl. Phys. Lett. **114**, 041107 (2019).

[60]S. Zhang, Z. Jin, Z. Zhu, W. Zhu, Z. Zhang, G. Ma, and J. Yao, "Bursts of efficient Terahertz radiation with saturation effect from metal-based ferromagnetic heterostructures," J. Phys. D

Appl. Phys. **51**, 034001 (2018).

[61]Y. Wu, M. Elyasi, X. Qiu, M. Chen, Y. Liu, L. Ke, and H. Yang, "High-performance THz emitters based on ferromagnetic/nonmagnetic heterostructures," Adv. Mater. **29**, 1603031 (2017).

[62]T. Seifert, U. Martens, S. Günther, M. A. W. Schoen, F. Radu, X. Z. Chen, I. Lucas, R. Ramos, M. H. Aguirre, P. A. Algarabel, A. Anadón, H. S. Körner, J. Walowski, C. Back, M. R. Ibarra, L. Morellón, E. Saitoh, M. Wolf, C. Song, K. Uchida, M. Münzenberga, I. Radu, and T. Kampfrath, "Terahertz spin currents and inverse spin Hall effect in thin-film heterostructures containing complex magnetic compounds," SPIN **7**, 1740010 (2017).

[63]T. J. Huisman and T. Rasing, "THz emission spectroscopy for THz spintronics," J. Phys. Soc. Jpn. **86**, 011009 (2017).

[64]Y. Sasaki, K. Z. Suzuki, and S. Mizukami, "Annealing effect on laser pulse-induced THz wave emission in Ta/CoFeB/MgO films," J. Phys. Soc. Jpn. **111**, 102401 (2017).

[65]T. J. Huisman, R. V. Mikhaylovskiy, J. D. Costa, F. Freimuth, E. Paz, J. Ventura, P. P. Freitas, S. Blügel, Y. Mokrousov, T. Rasing, and A. V. Kimel, "Femtosecond control of electric currents in metallic ferromagnetic heterostructures," Nat. Nanotechnol. **11**, 455 (2016).

[66]D. Yang, J. Liang, C. Zhou, L. Sun, R. Zheng, S. Luo, Y. Wu, and J. Qi, "Powerful and tunable THz emitters based on the Fe/Pt magnetic heterostructure," Adv. Opt. Mat. **4**, 1944 (2016).

[67]Y. Gao, Y. He, C. Pandey, T. Nie, C. Wang, D. Kong, B. Wang, L. Wen, C. Ruan, J. Miao, L. Wang, Y. Li, and W. Zhao, "Enhanced spintronic Terahertz emission in W/CoFeB heterostructures through annealing effect," 2019 44th International Conference on Infrared, Millimeter, and Terahertz Waves (IRMMW-THz), Paris, France , 1–3 (2019).

[68]M. B. Jungfleisch, Q. Zhang, W. Zhang, J. E. Pearson, R. D. Schaller, H. Wen, and A. Hoffmann, "Control of Terahertz emission by ultrafast spin-charge current conversion at Rashba interfaces," Phys. Rev. Lett. **120**, 207207 (2018).

[69]C. Zhou, Y. Liu, Z. Wang, S. Ma, M. Jia, R. Wu, L. Zhou, W. Zhang, M. Liu, Y. Wu, and J. Qi, "Broadband Terahertz generation via the interface inverse Rashba-Edelstein effect," Phys. Rev. Lett. **121**, 086801 (2018).

[70]V. M. Edelstein, "Spin polarization of conduction electrons induced by electric current in two-dimensional asymmetric electron systems," Solid State Commun. **73**, 233 (1990).

[71]S. I. Anisimov, B. L. Kapeliovich, and T. L. Perel'man, "Electron emission from metal surfaces exposed to ultrashort laser pulses," Sov. Phys. JETP **39**, 375 (1974).

[72]J. F. Ready, "Mechanism of electron emission produced by a giant-pulse laser," Phys. Rev. **137**, A620 (1965).

[73]M. Iannuzzi and R. Williamson, "Effects of absorption of laser radiation on metals," Nuovo Cimento **36**, 1130 (1965).

[74]G. Farkas, I. Kertèsz, Z. Nàray, and P. Varga, "On the intensity dependence of the non-linear electron emission from silver induced by a high power laser beam," Phys. Lett. A **24a**, 475 (1967).

[75]E. M. Logothetis and P. L. Hartman, "Laser-induced electron emission from solids: Many-photon photoelectric effects and thermionic emission," Phys. Rev. **187**, 460 (1969).

[76]F. V. Bunkin and A. M. Prokhorov, "Some features of the interaction between short laser radiation pulses and matter," Sov. Phys. JETP **25**, 1072 (1967).

[77]G. L. Eesley, "Observation of nonequilibrium electron heating in copper," Phys. Rev. Lett **51**, 2140 (1983).

[78]M. B. Agranat, A. A. Benditskii, G. M. Gandelman, A. G. Deviatkov, P. S. Kondratenko, B. I. Makshantsev, G. I. Rukman, and B. M. Stepanov, "Noninertial radiation from metals in interaction with ultrashort pulses of coherent infrared radiation," JETP Lett. **30**, 167 (1979).

[79]M. B. Agranat, A. A. Benditskir, G. M. Gandel'man, P. S. Kondratenko, B. I. Makshantsev, G. I. Rukman, and B. M. Stepanov, "Inertialess metal glow produced by picosecond pulses," Sov. Phys. JETP **52**, 27 (1980).

[80]A. Vaterlaus, D. Guarisco, M. Lutz, M. Aeschlimann, M. Stampanoni, and F. Meier, "Different spin and lattice temperatures observed by spin-polarized photoemission with picosecond laser pulses," J. Appl. Phys. **67**, 5661 (1990).

[81]M. B. Agranat, S. Ashitkov, A. Granovskii, and G. Rukman, "Interaction of picosecond laser pulses with the electron, spin, and phonon subsystems of nickel," Sov. Phys. JETP **59**, 804 (1984).

[82]A. Vaterlausa, T. Beutler, and F. Meier, "Spin-lattice relaxation time of ferromagnetic Gadolinium determined with time-resolved spin-polarized photoemission," Phys. Rev. Lett. **67**, 3314 (1991).

[83]J. Kerr, "On rotation of the plane of polarisation by reflection from the pole of a magnet," Philos. Mag. **3**, 321 (1877).

[84]R. L. Fork, C. V. Shank, C. Hirlimann, R. Yen, and W. J. Tomlinson, "Femtosecond white-light continuum pulses," Opt. Lett. **8**, 1 (1983).

[85]W. H. Knox, M. C. Downer, and C. V. Shank, "Amplified femtosecond optical pulses and continuum generation at 5-kHz repetition rate," Opt. Lett. **9**, 552 (1984).

[86]J. A. Valdmanis, R. L. Fork, and J. P. Gordon, "Generation of optical pulses as short as 27 femtoseconds directly from a laser balancing self-phase modulation, group-velocity dispersion, saturable absorption, and saturable gain," Opt. Lett. **10**, 131 (1985).

[87]R. W. Schoenlein, W. Z. Lin, J. G. Fujimoto, and G. L. Eesley, "Femtosecond studies of nonequilibrium electronic processes in metals," Phys. Rev. Lett. **58**, 1680 (1987).

[88]H. E. Elsayed-Ali, T. B. Norris, M. A. Pessot, and G. A. Mourou, "Time-resolved observation of electron-phonon relaxation in copper," Phys. Rev. Lett. **58**, 1212 (1987).

[89]E. Beaurepaire, J.-C. Merle, A. Daunois, and J.-Y. Bigot, "Ultrafast spin dynamics in ferromagnetic nickel," Phys. Rev. Lett. **76**, 4250 (1996).

[90]V. Cardin, T. Balciunas, K. Légaré, A. Baltuska, H. Ibrahim, E. Jal, B. Vodungbo, N. Jaouen, C. Varin, J. Lüning, and F. Légaré, "Wavelength scaling of ultrafast demagnetization in Co/Pt multilayers," Phys. Rev. B **101**, 054430 (2020).

[91]M. Matthiesen, D. Afanasiev, J. R. Hortensius, T. C. van Thiel, R. Medapalli, E. E. Fullerton, and A. D. Caviglia, "Temperature dependent inverse spin Hall effect in Co/Pt spintronic emitters," Appl. Phys. Lett. **116**, 212405 (2020).

[92]N. Moisan, G. Malinowski, J. Mauchain, M. Hehn, B. Vodungbo, J. Lüning, S. Mangin, E. E. Fullerton, and A. Thiaville, "Investigating the role of superdiffusive currents in laser induced demagnetization of ferromagnets with nanoscale magnetic domains," Sci. Rep. **4**, 4658 (2014).

[93]S. Mangin, M. Gottwald, C.-H. Lambert, D. Steil, V. Uhlíř, L. Pang, M. Hehn, S. Alebrand, M. Cinchetti, G. Malinowski, Y. Fainman, M. Aeschlimann, and E. E. Fullerton, "Engineered materials for all-optical helicity-dependent magnetic switching," Nat. Mat. **13**, 286 (2014).

[94]C.-H. Lambert, S. Mangin, B. S. D. C. S. Varaprasad, Y. K. Takahashi, M. Hehn, M. Cinchetti, G. Malinowski, K. Hono, Y. Fainman, M. Aeschlimann, and E. E. Fullerton, "All-optical control of ferromagnetic thin films and nanostructures," Science **345**, 1337 (2014).

[95]B. A. Ruzicka, K. Higley, L. K. Werake, and H. Zhao, "All-optical generation and detection of subpicosecond ac spin-current pulses in GaAs," Phys. Rev. B **78**, 045314 (2008).

[96]A. Melnikov, I. Razdolski, T. O. Wehling, E. T. Papaioannou, V. Roddatis, P. Fumagalli, O. Aktsipetrov, A. I. Lichtenstein, and U. Bovensiepen, "Ultrafast transport of laser-excited spin-polarised carriers in Au/Fe/MgO(001)," Phys. Rev. Lett. **107**, 076601 (2011).

[97]D. Rudolf, C. La-O-Vorakiat, M. Battiato, R. Adam, J. M. Shaw, E. Turgut, P. Maldonado, S. Mathias, P. Grychtola, H. T. Nembach, T. J. Silva, M. Aeschlimann, H. C. Kapteyn, M. M. Murnane, C. M. Schneider, and P. M. Oppeneer, "Ultrafast magnetization enhancement in metallic multilayers driven by superdiffusive spin current," Nat. Commun. **3**, 1037 (2012).

[98]G.-M. Choi, B.-C. Min, K.-J. Lee, and D. G. Cahill, "Spin current generated by thermally driven ultrafast demagnetization," Nat. Commun. **5**, 4334 (2014).

[99]S. O. Valenzuela and M. Tinkham, "Direct electronic measurement of the spin Hall effect," Nature **442**, 176 (2006).

[100]E. Saitoh, M. Ueda, and H. Miyajima, "Conversion of spin current into charge current at room temperature: Inverse spin-Hall effect," Appl. Phys. Lett. **88**, 182509 (2006).

[101]T. Kampfrath, M. Battiato, P. Maldonado, G. Eilers, J. Nötzold, S. Mährlein, V. Zbarsky, F. Freimuth, Y. Mokrousov, S. Blügel, M. Wolf, I. Radu, P. M. Oppeneer, and M. Münzenberg, "Terahertz spin current pulses controlled by magnetic heterostructures," Nat. Nanotechnol. **8**, 256 (2013).

[102]M. T. Hibberd, D. S. Lake, N. A. B. Johansson, T. Thomson, S. P. Jamison, and D. M. Graham, "Magnetic-field tailoring of the Terahertz polarization emitted from a spintronic source," Appl. Phys. Lett. **114**, 031101 (2019).

[103]M. Battiato, K. Carva, and P. M. Oppeneer, "Superdiffusive spin transport as a mechanism of ultrafast demagnetisation," Phys. Rev. Lett. **105**, 027203 (2010).

[104]G. E. W. Bauer, E. Saitoh, and B. J. van Wees, "Spin caloritronics," Nat. Mater. **11**, 391 (2012).

[105]M. Battiato, K. Carva, and P. M. Oppeneer, "Theory of laser-induced ultrafast superdiffusive spin transport in layered heterostructures," Phys. Rev. B **86**, 024404 (2012).

[106]T. S. Seifert, S. Jaiswal, J. Barker, S. T. Weber, I. Razdolski, J. Cramer, O. Gueckstock, S. F. Maehrlein, L. Nadvornik, S. Watanabe, C. Ciccarelli, A. Melnikov, G. Jakob, M. Münzenberg, S. T. B. Goennenwein, G. Woltersdorf, B. Rethfeld, P. W. Brouwer, M. Wolf, M. Kläui, and T. Kampfrath, "Femtosecond formation dynamics of the spin Seebeck effect revealed by Terahertz spectroscopy," Nat. Commun. **9**, 2899 (2018).

[107]A. Slachter, F. L. Bakker, J.-P. Adam, and B. J. van Wees, "Thermally driven spin injection from a ferromagnet into a non-magnetic metal," Nat. Phys. **6**, 879 (2010).

[108]K. Uchida, S. Takahashi, K. Harii, J. Ieda, W. Koshibae, K. Ando, S. Maekawa, and E. Saito, "Observation of the spin Seebeck effect," Nature **455**, 778 (2008).

[109]K. Uchida, H. Adachi, T. Ota, H. Nakayama, S. Maekawa, and E. Saitoh, "Observation of longitudinal spin-Seebeck effect in magnetic insulators," Appl. Phys. Lett. **97**, 172505 (2010).

[110]S. Rouzegar, L. Brandt, L. Nádvorník, D. Reiss, A. Chekhov, O. Gueckstock, C. In, M. Wolf, T. Seifert, P. Brouwer, G. Woltersdorf, and T. Kampfrath, "Laser-induced terahertz spin transport in magnetic nanostructures arises from the same force as ultrafast demagnetization," Cond-Mat.Mes-Hall , arXiv:2103.11710 (2021).

[111]A. Azevedo, L. H. Vilela-Leão, R. L. Rodríguez-Suárez, A. F. L. Santos, and S. M. Rezende, "Spin pumping and anisotropic magnetoresistance voltages in magnetic bilayers: Theory and experiment," Phys. Rev. B **83**, 144402 (2011).

[112]F. Guo, C. pandey, C. Wang, T. Nie, L. Wen, W. Zhao, J. Miao, L. Wang, and X. Wu, "Generation of highly efficient terahertz radiation in ferromagnetic heterostructures and its application in spintronic terahertz emission microscopy (STEM)," OSA Continuum **3**, 893 (2020).

[113]J. Walowski and M. Münzenberg, "Perspective: Ultrafast magnetism and THz spintronics," J. Appl. Phys. **120**, 140901 (2016).

[114]D. M. Nenno, R. Binder, and H. C. Schneider, "Simulation of hot-carrier dynamics and terahertz emission in laser-excited metallic bilayers," Phys. Rev. Appl. **11**, 054083 (2019).

[115]T. H. Dang, J. Hawecker, E. Rongione, G. B. Flores, D. Q. To, J. C. Rojas-Sanchez, H. Nong, J. Mangeney, J. Tignon, F. Godel, S. Collin, P. Seneor, M. Bibes, A. Fert, M. Anane, J.-M. George, L. Vila, M. Cosset-Cheneau, D. Dolfi, R. Lebrun, P. Bortolotti, K. Belashchenko, S. Dhillon, and H. Jaffrès, "Ultrafast spin-currents and charge conversion at $3d$-$5d$ interfaces probed by time-domain terahertz spectroscopy," Appl. Phys. Rev. **7**, 041409 (2020).

[116]B. Zaks, R. B. Liu, and M. S. Sherwin, "Experimental observation of electron-hole recollisions," Nature **483**, 580 (2012).

[117]T. Qi, Y.-H. Shin, K.-L. Yeh, K. A. Nelson, and A. M. Rappe, "Collective coherent control: Synchronization of polarization in ferroelectric $PbTiO_3$ by shaped THz fields," Phys. Rev. Lett. **102**, 247603 (2009).

[118]C. D. W. Mosley, M. Failla, D. Prabhakaran, and J. Lloyd-Hughes, "Terahertz spectroscopy of anisotropic materials using beams with rotatable polarization," Sci. Rep. **7**, 12337 (2017).

[119]H. Niwa, N. Yoshikawa, M. Kawaguchi, M. Hayashi, and R. Shimano, "Switchable generation of azimuthally- and radially-polarized terahertz beams from a spintronic terahertz emitter," Opt. Express **29**, 13331–13343 (2021).

[120]J. A. Deibel, K. Wang, M. D. Escarra, and D. M. Mittleman, "Enhanced coupling of Terahertz radiation to cylindrical wire waveguides," Opt. Express **14**, 279 (2006).

[121]H. Zhang, Z. Feng, J. Zhang, H. Bai, H. Yang, J. Cai, W. Zhao, W. Tan, F. Hu, B. Shen, and J. Sun, "Laser pulse induced efficient Terahertz emission from Co/Al heterostructures," Phys. Rev. B **102**, 024435 (2020).

[122]T. J. Huisman, C. Ciccarelli, A. Tsukamoto, R. V. Mikhaylovskiy, T. Rasing, and A. V. Kimel, "Spin-photo-currents generated by femtosecond pulses in a ferrimagnetic GdFeCo/Pt bilayer," Appl. Phys. Lett. **110**, 072402 (2017).

[123]G. Torosyan, S. Keller, L. Scheuer, R. Beigang, and E. T. Papaioannou, "Optimized spintronic Terahertz emitters based on epitaxial grown Fe/Pt layer structures," Sci. Rep. **8**, 1–9 (2018).

[124]G. Li, R. Medapalli, R. V. Mikhaylovskiy, F. E. Spada, T. Rasing, E. E. Fullerton, and A. V. Kimel, "THz emission from Co/Pt bilayers with varied roughness, crystal structure, and interface intermixing," Phys. Rev. Mat. **3**, 084415 (2019).

[125]X. Kozina, S. Ouardi, B. Balke, G. Stryganyuk, G. H. Fecher, C. Felser, S. Ikeda, H. Ohno, and E. Ikenaga, "A nondestructive analysis of the B diffusion in Ta-CoFeB-MgO-CoFeB-Ta magnetic tunnel junctions by hard X-ray photoemission," Appl. Phys. Lett. **96**, 072105 (2010).

[126]D. M. Nenno, L. Scheuer, D. Sokoluk, S. Keller, G. Torosyan, A. Brodyanski, J. Lösch, M. Battiato, M. Rahm, R. H. Binder, H. C. Schneider, R. Beigang, and E. T. Papaioannou, "Modification of spintronic Terahertz emitter performance through defect engineering," Sci. Rep. **9**, 13348 (2019).

[127]R. Schneider, M. Fix, J. Bensmann, S. M. de Vasconcellos, M. Albrecht, and R. Bratschitsch, "Spintronic GdFe/Pt THz emitters," Appl. Phys. Lett. **115**, 152401 (2019).

[128]M. Chen, R. Mishra, Y. Wu, K. Lee, and H. Yang, "Terahertz emission from compensated magnetic heterostructures," Adv. Opt. Mater. **6**, 1800430 (2018).

[129]J. Orehotsky and K. Schröder, "Magnetic properties of amorphous Fe_xGd_y alloy thin films," J. Appl. Phys. **43**, 2413 (1972).

[130]E. Kirk, C. Bull, S. Finizio, H. Sepehri-Amin, S. Wintz, A. K. Suszka, N. S. Bingham, P. Warnicke, K. Hono, P. W. Nutter, J. Raabe, G. Hrkac, T. Thomson, and L. J. Heyderman, "Anisotropy-induced spin reorientation in chemically modulated amorphous ferrimagnetic films," Phys. Rev. Mater. **4**, 074403 (2020).

[131]M. Fix, R. Schneider, J. Bensmann, S. M. de Vasconcellos, R. Bratschitsch, and M. Albrecht1, "Thermomagnetic control of spintronic THz emission enabled by ferrimagnets," Appl. Phys.

Lett. **116**, 012402 (2020).

[132]T. Hattori, K. Egawa, S. Ookuma, and T. Itatani, "Intense terahertz pulses from large-aperture antenna with interdigitated electrodes," Jpn. J. Appl. Phys. **45**, L422 (2006).

[133]Z. Feng, R. Yu, Y. Zhou, H. Lu, W. Tan, H. Deng, Q. Liu, Z. Zhai, L. Zhu, J. Cai, B. Miao, and H. Ding, "Highly efficient spintronic Terahertz emitter enabled by metal-dielectric photonic crystal," Adv. Opt. Mater. **6**, 1800965 (2018).

[134]X. Wang, L. Cheng, D. Zhu, Y. Wu, M. Chen, Y. Wang, D. Zhao, C. B. Boothroyd, Y. M. Lam, J. Zhu, M. Battiato, J. C. W. Song, H. Yang, and E. E. M. Chia, "Ultrafast spin-to-charge conversion at the surface of topological insulator thin films," Adv. Mater. **30**, 1802356 (2018).

[135]J. C. R. Sánchez, L. Vila, G. Desfonds, S. Gambarelli, J. P. Attané, J. M. D. Teresa, C. Magén, and A. Fert, "Spin-to-charge conversion using Rashba coupling at the interface between non-magnetic materials," Nat. Commun. **4**, 2944 (2013).

[136]Y. A. Bychkov and E. I. Rashba, "Properties of a 2D electron gas with lifted spectral degeneracy," JETP Lett. **39**, 78 (1984).

[137]R. Godfrey and M. Johnson, "Spin injection in mesoscopic silver wires: Experimental test of resistance mismatch," Phys. Rev. Lett. **96**, 136601 (2006).

[138]G. Li, R. V. Mikhaylovskiy, K. A. Grishunin, J. D. Costa, T. Rasing, and A. V. Kimel, "Laser induced THz emission from femtosecond photocurrents in Co/ZnO/Pt and Co/Cu/Pt multilayers," J. Phys. D Appl. Phys. **51**, 134001 (2018).

[139]P. Yang, Q. Shao, G. Yu, C. He, K. Wong, X. Lu, J. Zhang, B. Liu, H. Meng, L. He, K. L. Wang, and Y. Xu, "Enhancement of the spin–orbit torque efficiency in W/Cu/CoFeB heterostructures via interface engineering," Appl. Phys. Lett. **117**, 082409 (2020).

[140]S. N. Panda, S. Mondal, J. Sinha, S. Choudhury, and A. Barman, "All-optical detection of interfacial spin transparency from spin pumping in β-Ta/CoFeB thin films," Sci. Adv. **5**, 2375 (2019).

[141]W.-T. Lu, Y. Zhao, M. Battiato, Y. Wu, and Z. Yuan, "Interface reflectivity of a superdiffusive spin current in ultrafast demagnetization and terahertz emission," Phys. Rev. B. **101**, 014435 (2020).

[142]Y. Ogasawara, Y. Sasaki, S. Iihama, A. Kamimaki, K. Z. Suzuki, and S. Mizukami, "Laser-induced Terahertz emission from layered synthetic magnets," Appl. Phys. Express **13**, 063001 (2020).

[143]Q. Zhang, Y. Yang, Z. Luo, Y. Xu, R. Nie, X. Zhang, and Y. Wu, "Terahertz emission from an exchange-coupled synthetic antiferromagnet," Phys. Rev. Appl. **13**, 054016 (2020).

[144]H. Zhong, S. Qiao, S. Yan, L. Liang, Y. Zhao, and S. Kang, "Terahertz spin-transfer torque oscillator based on a synthetic antiferromagnet," J. Magn. Magn. Mater. **497**, 166070 (2020).

[145]P. Bruno and C. Chappert, "Oscillatory coupling between ferromagnetic layers separated by a nonmagnetic metal spacer," Phys. Rev. Lett. **67**, 1602 (1991).

[146]S. S. Parkin and D. Mauri, "Spin engineering: Direct determination of the Ruderman-Kittel-Kasuya-Yosida far-field range function in Ruthenium," Phys. Rev. B **44**, 7131 (1991).

[147]H. J. Waring, N. A. B. Johansson, I. J. Vera-Marun, and T. Thomson, "Zero-field optic mode beyond 20 GHz in a synthetic antiferromagnet," Phys. Rev. Appl. **13**, 034035 (2020).

[148]Q. Zhang, Z. Luo, H. Li, Y. Yang, X. Zhang, and Y. Wu, "Terahertz emission from anomalous Hall effect in a single-layer ferromagnet," Phys. Rev. Appl. **12**, 054027 (2019).

[149]Y. Yang, Z. Luo, H. Wu, Y. Xu, R.-W. Li, S. J. Pennycook, S. Zhang, and Y. Wu, "Anomalous Hall magnetoresistance in a ferromagnet," Nat. Commun. **9**, 2255 (2018).

[150]J. Smit, "The spontaneous Hall effect in ferromagnetics," Physica **21**, 877 (1955).

[151]L. Berger, "Side-jump mechanism for the Hall effect of ferromagnets," Phys. Rev. B-Solid State **2**, 4559 (1970).

[152]R. Karplus and J. M. Luttinger, "Hall effect in ferromagnetics," Phys. Rev. **95**, 1154 (1954).

[153]T. Löffler, M. Kreß, M. Thomson, T. Hahn, N. Hasegawa, and H. G. Roskos, "Comparative performance of terahertz emitters in amplifier-laser-based systems," Semicond. Sci. Technol. **20**, S134 (2005).

[154]C. Kealhofer, W. Schneider, D. Ehberger, A. Ryabov, F. Krausz, and P. Baum, "All-optical control and metrology of electron pulses," Science **352**, 429 (2016).

[155]E. Liu, Y. Sun, N. Kumar, L. Muechler, A. Sun, L. Jiao, S.-Y. Yang, D. Liu, A. Liang, Q. Xu, J. Kroder, V. Süß, H. Borrmann, C. Shekhar, Z. Wang, C. Xi, W. Wang, W. Schnelle, S. Wirth, Y. Chen, S. T. B. Goennenwein, and C. Felser, "Giant anomalous Hall effect in a ferromagnetic kagome-lattice semimetal," Nature Physics **14**, 1125 (2018).

[156]O. V. Kotov and Y. E. Lozovik, "Giant tunable nonreciprocity of light in weyl semimetals," Phys. Rev. B **98**, 195446 (2018).

[157]W. X. R, "Anomalous spin hall and inverse spin hall effects in magnetic systems," Commun. Phys. **4**, 55 (2021).

[158]X. Chen, H. Wang, C. Wang, C. Ouyang, G. Wei, T. Nie, W. Zhao, J. Miao, Y. Li, L. Wang, and X. Wu, "Efficient generation and arbitrary manipulation of chiral Terahertz waves emitted from Bi_2Te_3–Fe heterostructures," Adv. Photonics Res. **n/a**, 2000099 (2021).

[159]L. Cheng, X. Wang, W. Yang, J. Chai, M. Yang, M. Chen, Y. Wu, X. Chen, D. Chi, K. E. J. Goh, J.-X. Zhu, H. Sun, S. Wang, J. C. W. Song, M. Battiato, H. Yang, and E. E. M. Chia, "Far out-of-equilibrium spin populations trigger giant spin injection into atomically thin MoS_2," Nat. Phys. **15**, 347–351 (2019).

[160]J. D. Costa, T. J. Huisman, R. V. Mikhaylovskiy, I. Razdolski, J. Ventura, J. M. Teixeira, D. S. Schmool, G. N. Kakazei, S. Cardoso, P. P. Freitas, T. Rasing, and A. V. Kimel, "Terahertz dynamics of spins and charges in CoFe/Al_2O_3 multilayers," Phys. Rev. B **91**, 104407 (2015).

[161]E. Beaurepaire, G. M. Turner, S. M. Harrel, M. C. Beard, J.-Y. Bigot, and C. A. Schmuttenmaer, "Coherent Terahertz emission from ferromagnetic films excited by femtosecond laser pulses," Appl. Phys. Lett. **84**, 3465–3467 (2004).

[162]J. Nishitani, K. Kozuki, T. Nagashima, and M. Hangyo, "Terahertz radiation from coherent antiferromagnetic magnons excited by femtosecond laser pulses," Appl. Phys. Lett. **96**, 221906 (2010).

[163]T. J. Huisman, R. V. Mikhaylovskiy, T. Rasing, A. V. Kimel, A. Tsukamoto, B. de Ronde, L. Ma, W. J. Fan, and S. M. Zhou, "Sub-100-ps dynamics of the anomalous Hall effect at Terahertz frequencies," Phys. Rev. B. **95**, 094418 (2017).

[164]X. Zhou, B. Song, X. Chen, Y. You, S. Ruan, H. Bai, W. Zhang, G. Ma, J. Yao, F. Pan, Z. Jin, and C. Song, "Orientation-dependent THz emission in non-collinear antiferromagnetic Mn_3Sn and Mn_3Sn-based heterostructures," Appl. Phys. Lett. **115**, 182402 (2019).

[165]Y. Gao, S. Kaushik, E. J. Philip, Z. Li, Y. Qin, Y. P. Liu, W. L. Zhang, Y. L. Su, X. Chen, H. Weng, D. E. Kharzeev, M. K. Liu, and J. Qi, "Chiral Terahertz wave emission from the Weyl semimetal TaAs," Nat. Commun. **11**, 720 (2020).

[166]O. Gueckstock, L. Nádvorník, M. Gradhand, T. S. Seifert, G. Bierhance, R. Rouzegar, M. Wolf, M. Vafaee, J. Cramer, M. A. Syskaki, G. Woltersdorf, I. Mertig, G. Jakob, M. Kläui, and T. Kampfrath, "Terahertz spin-to-charge conversion by interfacial skew scattering in metallic bilayers," Adv. Mater. **33**, 2006281 (2021).

[167]J. Shen, X. Fan, Z. Chen, M. F. DeCamp, H. Zhang, and J. Q. Xiao, "Damping modulated Terahertz emission of ferromagnetic films excited by ultrafast laser pulses," Appl. Phys. Lett. **101**, 072401 (2012).

[168]H. Qiu, L. Zhou, C. Zhang, J. Wu, Y. Tian, S. Cheng, S. Mi, H. Zhao, Q. Zhang, D. Wu, B. Jin, J. Chen, and P. Wu, "Ultrafast spin current generated from an antiferromagnet," Nat. Phys. (2020).

[169]T. Kampfrath, M. Battiato, A. Sell, F. Freimuth, A. Leitenstorfer, M. Wolf, R. Huber, P. M. Oppeneer, and M. Münzenberg, "Ultrafast spin precession and transport controlled and probed with Terahertz radiation," in *Proc. SPIE*, Vol. 8984 (2014).

[170]R. D. Averitt, "Getting current pulses under control," Nat. Nanotechnol. **8**, 232–233 (2013).

[171]D. Khusyainov, S. Ovcharenko, M. Gaponov, A. Buryakov, A. Klimov, N. Tiercelin, P. Pernod, V. Nozdrin, E. Mishina, A. Sigov, and V. Preobrazhensky, "Polarization control of THz emission using spin-reorientation transition in spintronic heterostructure," Sci. Rep. **11**, 1–8 (2021).

[172]Y. Sasaki, Y. Kota, S. Iihama, K. Z. Suzuki, A. Sakuma, and S. Mizukami, "Effect of Co and Fe stoichiometry on Terahertz emission from Ta/$(Co_xFe_{1-x})_{80}B_{20}$/MgO thin films," Phys. Rev. B. **100**, 140406 (2019).

[173]R. Adam, G. Chen, D. E. Bürgler, T. Shou, I. Komissarov, S. Heidtfeld, H. Hardtdegen, M. Mikulics, C. M. Schneider, and R. Sobolewski, "Magnetically and optically tunable Terahertz radiation from Ta/NiFe/Pt spintronic nanolayers generated by femtosecond laser pulses," Appl. Phys. Lett. **114**, 212405 (2019).

[174]S.-C. Chen, Z. Feng, J. Li, W. Tan, L.-H. Du, J. Cai, Y. Ma, K. He, H. Ding, Z.-H. Zhai, Z.-R. Li, C.-W. Qiu, X.-C. Zhang, and L.-G. Zhu, "Ghost spintronic THz-emitter-array microscope," Light: Sci. Appl. **9**, 99 (2020).

[175]M. Chen, Y. Wu, Y. Liu, K. Lee, X. Qiu, P. He, J. Yu, and H. Yang, "Current-enhanced broadband THz emission from spintronic devices," Adv. Opt. Mater. **7**, 1801608 (2019).

[176]T. S. Seifert, N. M. Tran, O. Gueckstock, S. M. Rouzegar, L. Nadvornik, S. Jaiswal, G. Jakob, V. V. Temnov, M. Münzenberg, M. Wolf, M. Kläui, and T. Kampfrath, "Terahertz spectroscopy for all-optical spintronic characterization of the spin-Hall-effect metals Pt, W and $Cu_{80}Ir_{20}$," J. Phys. D: Appl. Phys. **51**, 364003 (2018).

[177]D. Kong, X. Wu, B. Wang, T. Nie, M. Xiao, C. Pandey, Y. Gao, L. Wen, W. Zhao, C. Ruan, J. Miao, Y. Li, and L. Wang, "Broadband spintronic Terahertz emitter with magnetic field manipulated polarizations," Adv. Optical Mater. **7**, 1900487 (2019).

[178]B. Wang, S. Shan, X. Wu, C. Wang, C. Pandey, T. Nie, W. Zhao, Y. Li, J. Miao, and L. Wang, "Picosecond nonlinear spintronic dynamics investigated by Terahertz emission spectroscopy," Appl. Phys. Lett. **115**, 121104 (2019).

[179]Z. Jin, S. Zhang, W. Zhu, Q. Li, W. Zhang, Z. Zhang, S. Lou, Y. Dai, X. Lin, G. Ma, and J. Yao, "Terahertz radiation modulated by confinement of picosecond current based on patterned ferromagnetic heterostructures," Phys. Status Solidi RRL **13**, 1900057 (2019).

[180]F. Guo, C. pandey, C. Wang, T. Nie, L. Wen, W. Zhao, J. Miao, L. Wang, and X. Wu, "Generation of highly efficient Terahertz radiation in ferromagnetic heterostructures and its application in spintronic Terahertz emission microscopy (STEM)," OSA Continuum **3**, 893–902 (2020).

[181]U. Nandi, M. S. Abdelaziz, S. Jaiswal, G. Jakob, O. Gueckstock, S. M. Rouzegar, T. S. Seifert, M. Kläui, T. Kampfrath, and S. Preu, "Antenna-coupled spintronic Terahertz emitters driven by a 1550 nm femtosecond laser oscillator," Appl. Phys. Lett. **115**, 022405 (2019).

[182]X. Chen, X. Wu, S. Shan, F. Guo, D. Kong, C. Wang, T. Nie, C. Pandey, L. Wen, W. Zhao, C. Ruan, J. Miao, Y. Li, and L. Wang, "Generation and manipulation of chiral broadband Terahertz waves from cascade spintronic Terahertz emitters," Appl. Phys. Lett. **115**, 221104 (2019).

[183]P. Agarwal, R. Medwal, A. Kumar, H. Asada, Y. Fukuma, R. S. Rawat, M. Battiato, and R. Singh, "Ultrafast photo-thermal switching of Terahertz spin currents," Adv. Funct. Mater. , 2010453 (2021).

[184]M. Fix, R. Schneider, S. M. de Vasconcellos, R. Bratschitsch, and M. Albrecht, "Spin valves as magnetically switchable spintronic THz emitters," Appl. Phys. Lett. **117**, 132407 (2020).

[185]B. René, P. E. Th, S. Laura, K. Sascha, T. Garik, R. Marco, S. Dominik, T. Miezel, O. Yoshinori, K. Hideaki, A. Jessica, M. u. Valynn Katrine, and T. Masahiko, "Efficient Terahertz generation using Fe/Pt spintronic emitters pumped at different wavelengths," in *Proc. SPIE*, Vol. 10917 (2019).

[186]E. T. Papaioannou, G. Torosyan, S. Keller, L. Scheuer, M. Battiato, V. K. Mag-Usara, J. L'huillier, M. Tani, and R. Beigang, "Efficient Terahertz generation using Fe/Pt spintronic emitters pumped at different wavelengths," IEEE Trans. Magn. **54**, 1–5 (2018).

[187]P. Stremoukhov, A. Safin, M. Logunov, S. Nikitov, and A. Kirilyuk, "Spintronic Terahertz-frequency nonlinear emitter based on the canted antiferromagnet-platinum bilayers," J. Appl. Phys. **125**, 223903 (2019).

[188]T. H. Dang, J. Hawecker, E. Rongione, G. B. Flores, D. Q. To, J. C. Rojas-Sanchez, H. Nong, J. Mangeney, J. Tignon, F. Godel, S. Collin, P. Seneor, M. Bibes, A. Fert, M. Anane, J.-M. George, L. Vila, M. Cosset-Cheneau, D. Dolfi, R. Lebrun, P. Bortolotti, K. Belashchenko, S. Dhillon, and H. Jaffrès, "Ultrafast spin-currents and charge conversion at 3d-5d interfaces

probed by time-domain Terahertz spectroscopy," Appl. Phys. Rev. **7**, 041409 (2020).

[189]H. S. Qiu, K. Kato, K. Hirota, N. Sarukura, M. Yoshimura, and M. Nakajima, "Layer thickness dependence of the Terahertz emission based on spin current in ferromagnetic heterostructures," Opt. Express. **12**, 15247 (2018).

[190]H. Qiu, L. Wang, Z. Shen, K. Kato, N. Sarukura, M. Yoshimura, W. Hu, Y. Lu, and M. Nakajima, "Magnetically and electrically polarization-tunable THz emitter with integrated ferromagnetic heterostructure and large-birefringence liquid crystal," Appl. Phys. Exp. **11**, 092101 (2018).

[191]Y. Sasaki, Y. Takahashi, and S. Kasai, "Laser-induced Terahertz emission in Co_2MnSi¶t structure," Appl. Phys. Express **13**, 093003 (2020).

[192]B. Song, Y. Song, S. Zhang, K. Jin, W. Zhu, Q. Li, Z. Zhang, X. Lin, Y. Dai, X. Yan, G. Ma, Z. Jin, and J. Yao, "Controlling Terahertz radiation with subwavelength blocky patterned CoFeB/Pt heterostructures," Appl. Phys. Express **12**, 122003 (2019).

[193]L. Sergi, L. Yi, W. Weipeng, K. M. Taghipour, Z. Qi, Z. Wei, E. P. John, D. Ralu, D. S. Richard, H. Axel, W. Haidan, and J. M. Benjamin, "Terahertz emission from magnetic thin film and patterned heterostructures," in *Proc. SPIE*, Vol. 11090 (2019).

[194]Y. Sasaki, G. Li, T. Moriyama, T. Ono, R. V. Mikhaylovskiy, A. V. Kimel, and S. Mizukami, "Laser stimulated THz emission from Pt/CoO/FeCoB," Appl. Phys. Lett. **117**, 192403 (2020).

[195]C. Yu and S. Liu, "Electronic-spintronic Terahertz emitter," Phys. Rev. Appl. **11**, 024055 (2019).

[196]R. Schneider, M. Fix, R. Heming, S. M. de Vasconcellos, M. Albrecht, and R. Bratschitsch, "Magnetic-field-dependent THz emission of spintronic TbFe/Pt layers," ACS Photonics. **5**, 3936–3942 (2018).

[197]O. Panahi, B. Yahyaei, S. M. Mousavi, and A. M. Ghiasabadi, "High performance Terahertz emitter based on inverse spin Hall effect in metallic Fe/Au heterostructure," Laser Phys. **30**, 055001 (2020).

[198]B. C. Choi, J. Rudge, K. Jordan, and T. Genet, "Terahertz excitation of spin dynamics in ferromagnetic thin films incorporated in metallic spintronic-THz-emitter," Appl. Phys. Lett. **116**, 132406 (2020).

[199]M. Tong, Y. Hu, Z. Wang, T. Zhou, X. Xie, X. Cheng, and T. Jiang, "Enhanced Terahertz radiation by efficient spin-to-charge conversion in Rashba-mediated Dirac surface states," Nano Lett. **21**, 60–67 (2020).

[200]Q. Zhang, D.Hong, C. Liu, R. Schaller, D. Fong, A. Bhattacharya, and H. Wen, "Gate-tunable Terahertz emission at oxide interfaces via ultrafast spin-to-charge current conversion," 2019 Conference on Lasers and Electro-Optics (CLEO), San Jose, California United States. , FM4D.7 (2019).

[201]E. Vetter, M. Biliroglu, D. Seyitliyev, P. Reddy, R. Kirste, Z. Sitar, R. Collazo, K. Gundogdu, and D. Sun, "Observation of carrier concentration dependent spintronic Terahertz emission from n-GaN/NiFe heterostructures," Appl. Phys. Lett. **117**, 093502 (2020).

FIG. 1. Table comparing the characteristics of commonly used THz emitters in THz-TDS. For each tick the reference, R, indicates the references that demonstrated achievement of the particular source characteristic, as follows: R1:[17]; R2:[15,16]; R3:[12–16]; R4:[22–24]; R5:[5,26,27]; R6:[5,25,26,28]; R7:[33]; R8:[36,37]; R9:[39]; R10:[38]; R11:[38]; R12:[39–41]; R13:[40,41]; R14:[42]; R15:[39,41]; R16:[41]; R17:[47]; R18:[48,49]; R19:[48,49]; R20:[58]; R21:[57,58]; R22:[57,58]; R23:[57].

FIG. 2. Generation of THz radiation from a spintronic bilayer structure composed of a ferromagnetic (FM), thin film and a non-magnetic (NM) thin film. A femtosecond laser pump pulse induces a spin-polarized current ($\boldsymbol{j}_s$) in the FM layer that propagates across the FM/NM interface to the NM layer where it is converted to a transverse charge current ($\boldsymbol{j}_c$) by the inverse spin-Hall effect (ISHE). The induced charge current, propagating in the plane of the NM layer, results in the emission of a pulse of THz radiation, $\boldsymbol{E}_{THz}$, that is polarized perpendicular to the direction of the applied magnetic field (H), and hence magnetization direction ($\mathbf{M}$) of the FM layer. For illustrative purposes the moment of the individual spins are shown by the red and blue arrows. The relative directions of $\mathbf{M}, \boldsymbol{j}_s, \boldsymbol{j}_c$ and $\boldsymbol{E}_{THz}$ are highlighted in the side view diagrams. These directions are independent of the pump pulse polarization.

FIG. 4. (a) Transient remnant longitudinal MOKE hysteresis signal of a Ni (20 nm)/MgF_2 (100 nm) film, illuminated using a pump with fluence = 7 mJ cm^{-2}. (b) Calculated electron, T_e, spin, T_S, and lattice, T_i, temperatures. Images are reproduced with permission from Beaurepaire *et al.*[89]

FIG. 5. The spin-dependent Seebeck effect across a FM/NM interface. An applied field, H_{app}, saturates the FM layer to align its magnetization perpendicular to the direction of the heat current. The heat current travelling across the FM/NM interface induces a spin imbalance proportional to $\mu_\uparrow$ - $\mu_\downarrow$, which relaxes in the FM and NM layers on the length scale of their spin-relaxation lengths λ_{FM} and λ_{NM}, respectively. Image redrawn from Slachter *et al.*[107]

FIG. 6. A pump laser generates a heat current in the Pt layer which diffuses to the FM_1 layer, driving the demagnetization of the FM_1 layer with perpendicular anisotropy. The demagnetization generates a diffusive spin current which traverses the FM_1/Cu interface. This thermally-driven current is absorbed by the in-plane FM_2 layer. STT tilts the magnetization of the FM_2 layer out of plane, inducing precession.[98] Image reproduced with permission from Choi *et al.*[98]

FIG. 7. Example of a method used by Hibberd *et al.*[102] to control the polarization profile of the THz pulses of radiation emitted from $Ni_{80}Fe_{20}$/Pt bilayers. Two permanent magnets have been used to apply a magnetic field pattern to the spintronic source, where (a) and (c) show the magnetic field lines produced when magnets are orientated with aligned and opposing polarity, respectively. The corresponding linear and quadrupolar THz electric field lines are shown in (b) and (d). Image reproduced with permission from Hibberd *et al.*[102]

FIG. 3. Transient picosecond thermomodulation spectra for Cu. Image reproduced with permission from Eesley.[77] Time resolved $\Delta R/R$ transients are plotted for four probe beam photon energies: 2.10 eV, 2.13 eV, 2.15 eV and 2.16 eV.

FIG. 8. Table showing number of papers published for different material combinations in spintronic THz emitters (as of March 2021). Columns represent NM layer (layer 1) materials investigated, including topological insulators, semiconductors and magnetic materials. Rows represent magnetic materials investigated for the FM layer (layer 2) including ferromagnetic, ferrimagnetic and antiferromagnetic thin films. Colormap indicates the number of unique papers published that investigate each material combination. Symbols denote whether investigated material combinations are bilayer (red circle), trilayer (blue triangle) or multilayer (green square) THz emitters. R denotes the references that investigate each material combination, as follows: R1:[158]; R2:[148]; R3:[61,65,159]; R4:[160]; R5:[89,161]; R6:[162]; R7:[163]; R8:[164]; R9:[165]; R10:[166]; R11:[121,166]; R12:[68]; R13:[103] R14:[166,167]; R15:[57,63]; R16:[161]; R17:[61,65,121,138,166]; R18:[168]; R19:[106]; R20:[101,169,170]; R21:[143]; R22:[61,65]; R23:[60,171]; R24:[60]; R25:[57,60,63]; R26:[69]; R27:[61]; R28:[57,60,63,64,142,172]; R29:[167,173]; R30:[133,174]; R31:[61,175]; R32:[57–59,63,67,158,176–182]; R33:[183]; R34:[131,133]; R35:[57,63,142]; R36:[57,66,123,126,133,166,174,184–186]; R37:[187]; R38:[62]; R39:[57,61,65,66,91,121,124,138,166,175,188–190]; R40:[57,191]; R41:[57–59,61–63,67,126,158,176–182,192–194]; R42:[128]; R43:[194]; R44:[191]; R45:[57,66,195]; R46:[57,102,166,173,183,188]; R47:[62,127,131]; R48:[122]; R49:[128,184]; R50:[106,168]; R51:[127,196]; R52:[101,169,170,197,198]; R53:[65]; R54:[199]; R55:[176]; R56:[200]; R57:[126,199]; R58:[159]; R59:[138]; R60:[201]; R61:[171]

FIG. 9. Emission of THz radiation from NM/FM heterostructures, reproduced with permission from Kampfrath *et al.*[101] (a) Measured signal, $S_x(t)$, of THz pulse emitted from Fe/Ru and Fe/Au bilayers. Reversal of the sample magnetization inverts the THz pulse (dark to light curves). (b) Transient THz electric field amplitude, $|E_x(\omega)|$, calculated by Fourier transformation of the THz field, $E_x(t)$.

FIG. 10. THz pulse amplitude emitted from $Co_{20}Fe_{60}B_{20}$ (3 nm)/NM (3 nm) bilayers (red bars), excited by fs pulses from a Ti:sapphire laser (duration 10 fs, wavelength 800 nm, pulse energy 2.5 nJ, repetition rate 80 MHz). The calculated values of the spin-Hall conductivity are shown for comparison (blue bars). Image reproduced with permission from Seifert *et al.*[57]

FIG. 11. THz pulse waveforms emitted from NM (4 nm)/Co (4 nm) bilayers excited by fs pulses from a Ti:sapphire laser (duration 120 fs, wavelength 800 nm). The NM layers are a) Pt, b) Ir, c) Gd, d) Ru, e) Ta and f) W. The bilayers were capped with 4 nm of SiO_2 to prevent oxidation of the FM layer. Image reproduced with permission from Wu *et al.*[61]

FIG. 12. Measured signal of the THz pulse emitted from FM (3 nm)/Pt (3 nm) bilayers, excited by fs pulses from a Ti:sapphire laser (duration 10 fs, wavelength 800 nm, pulse energy 2.5 nJ, repetition rate 80 MHz). Image reproduced with permission from Seifert *et al.*[57]

FIG. 13. Measured signal of the THz pulse emitted from $Co_{20}Fe_{60}B_{20}$/Pt bilayers (from various research institutions) as a function of the total bilayer thickness, d_{tot}. THz-TDS was performed using fs laser pulses of duration 10 fs, wavelength 800 nm, pulse energy 2.5 nJ and repetition rate 80 MHz. Image reproduced with permission from Seifert *et al.*[57]

FIG. 14. Peak THz electric field amplitude from Co/Pt heterostructures, excited using a 40 fs circularly polarized 800 nm laser with pulse energy 20 μJ. Material properties of the heterostructures are varied by adjusting the Ar pressure of the Co layer during deposition, growing the bilayers onto glass or Cr-buffered MgO substrates, and including a Co_xPt_{1-x} alloy spacer layer. Table produced from data provided in Li *et al.*[124]

FIG. 15. (a) Peak values of THz pulse amplitudes emitted from Ta/CoFeB/MgO/Ta heterostructures as a function of CoFeB thickness, t_{CFB}, for annealing temperatures, T_a. Heterostructures were excited using a 120 fs pulsed, Ti:Sapphire laser with a central wavelength of 800 nm, repetition rate of 1 kHz and fluence of 1.1 mJ cm^{-2}. (b) Calculated data for the emitted THz radiation versus t_{CFB}. Image reproduced with permission from Sasaki *et al.*[64]

FIG. 16. HR-EFTEM images of Fe/Pt bilayers grown onto (001)-plane MgO substrates. (a) Pt layer deposited at T_{dep} = 300°C and (b) Pt layer deposited at T_{dep} = RT. Image reproduced with permission from Nenno *et al.*[126]

FIG. 17. Peak-to-peak THz pulse amplitudes emitted from Gd_xFe_{1-x}/Pt bilayers as a function of Gd content x, excited using a 1 kHz laser amplifier system with a central wavelength of 800 nm and pulse duration of 60 fs. Blue dots (red triangles) correspond to measured (modelled) data. Image reproduced with permission from Schneider *et al.*[127]

FIG. 18. Measured THz electric field of a GdFeCo/Pt bilayer as a function of applied, in-plane magnetic field for a temperature of 155 K and 295 K. Image reproduced with permission from Huisman *et al.*[122]

FIG. 19. Excitation of the heterostructure with an 800 nm wavelength, 60 fs laser pulse (fluence = 0.75 mJ cm^{-2}) enables the generation of spin currents by Fe electrons in the Gd_xFe_{1-x} layers. In the NM layers, spin currents are converted to charge currents $\boldsymbol{j}_c$ by the ISHE. The orientation of the Fe magnetic moments in the $Gd_{30}Fe_{70}$ layer is manipulated by the temperature of the heterostructure, where temperatures below T_{comp} produce the high-amplitude THz radiation emitting state (a), and temperatures above T_{comp} produce the low-amplitude THz radiation emitting state (b). Image reproduced with permission from Fix *et al.*[131]

FIG. 20. Fourier spectra of THz signal (grey), transient THz electric field (red), and spectral phase (blue circles) emitted from a W (1.8 nm)/$Co_{20}Fe_{60}B_{20}$ (2.0 nm)/Pt (1.8 nm) trilayer using a 5.5 mJ pulsed laser with central wavelength 800 nm, duration 40 fs and repetition rate 1 kHz. Note that spectral features, such as the decrease in THz pulse amplitude at 8 THz, arise from the 10 μm thick ZnTe electro-optic detector which was used in this experiment and not from the emitter. Image reproduced with permission from Seifert *et al.*[58]

FIG. 21. (a) THz waveforms measured for [Pt (2 nm)/Fe (1 nm)/MgO (2 nm)]$_n$ cascaded multilayers (n = 1,3,5,7). (b) THz waveforms measured for the structure with n = 3 repeated layers and a 100 μm GaP crystal. All spectra were obtained at the same pump laser fluence of 200 μJ cm^{-2}, generated by a Ti:Sapphire amplifier with central wavelength 800 nm, duration 55 fs and repetition rate 1 kHz. Image reproduced with permission from Yang *et al.*[66]

FIG. 22. The inverse Rashba-Edelstein effect (IREE). (a) Injection of spin current, $\boldsymbol{j}_s$, into an interfacial Rashba system can cause a shift in the Fermi surface contours by Δk. (b) A FM/NM/NM heterostructure with a Rashba interface (e.g. CoFeB/Ag/Bi[68]) subjected to $\boldsymbol{j}_s$ leads to an unequal spin accumulation at the NM_1/NM_2 interface. The shift in Fermi surface contours gives rise to a charge current, $\boldsymbol{j}_c^{IREE}$ at the Rashba interface.

FIG. 23. Generation of HD THz radiation from a Co (10 nm)/Pt (2 nm) bilayer. (a) A circularly polarized fs laser pump induces a spin-polarized current (j) in the FM layer which is converted to a charge current, n, at the FM layer/NM layer interface by the IREE spin-to-charge current conversion mechanism. This generates a pulse of THz radiation polarized parallel to the magnetization of the FM layer $\mathbf{M}$. (b) Measured electric field of the emitted pulses of HD THz radiation, $|E_y|$, for opposite helicities of light, σ^+ and σ^-, measured using 50 fs, circularly polarized laser pulses with a central wavelength of 800 nm. Image reproduced with permission from Huisman *et al.*[65]

FIG. 24. FMR spectrum (top) and corresponding field dependence of the charge current (bottom) for (a) NiFe (15 nm)/Ag (10 nm), (b) NiFe (15 nm)/Bi (8 nm) and (c) NiFe (15 nm)/Ag (5 nm)/Bi (8 nm) heterostructures, measured by FMR and electrical measurement techniques. Measurements were performed using a resonator cavity with a frequency $\sim$9.5 GHz. Image reproduced with permission from Rojas Sánchez *et al.*[135]

FIG. 25. Measured THz waveforms for a Pt(2 nm)/Co (3 nm) heterostructure (orange), Pt(6 nm)/Co (3 nm) green and Bi_2Se_3 (10 nm)/Co (3 nm) heterostructure (blue), measured at RT using a 60 mW laser with central wavelength 800 nm, duration 50 fs and repetition rate 1 kHz. Image reproduced with permission from Wang *et al.*[134]

FIG. 26. Integrated strength of the (a,b) helicity dependent, and (c,d) helicity independent (HI) THz electric field as a function of thickness for Cu (a,c) and ZnO (b,d) interlayers. Emission spectra were obtained using circularly polarized laser pulses with central wavelength 800 nm, duration 40 fs, repetition rate 500 Hz and the same fluence of 0.6 mJ cm^{-2}. Insets in figures (b) and (d) show time-resolved traces of the HI THz electric field, measured as a function of ZnO thickness. Images reproduced with permission from Li *et al.*[138]

FIG. 27. (a) Schematic diagram of the induced spin current, $\boldsymbol{j}_s$, and charge current, $\boldsymbol{j}_c$, pulses sourcing the THz emission in the antiparallel and parallel aligned synthetic (anti)ferromagnetic structures. A 120 fs laser with a central wavelength of 800 nm and a fluence of 1 mJ cm^{-2} was used to excite the structures in this study.[142] (b) THz emission as a function of time from Ta/CoFeB/Ir/CoFeB/Ta films with d_s = 0.5 nm and 0.9 nm, reproduced with permission from Ogasawara *et al.*[142] Black triangles correspond to THz emission in the absence of an applied field, whereas blue (empty) circles and red (solid) circled correspond to emission when H_{app} = +/-1.3 T, respectively.

FIG. 28. The anomalous spin-Hall effect in a thin ferromagnetic layer. On the application of longitudinal current, I, spin-up ($\uparrow$) and spin-down ($\downarrow$) electrons are deflected to the boundaries of the FM layer, leading to the generation of a transverse charge current, $\boldsymbol{j}_c$, and spin current, $\boldsymbol{j}_s$, perpendicular to the magnetization, $\mathbf{M}$, gives rise to the anomalous Hall voltage, V_H, across the FM layer.

FIG. 29. (a) Schematic of the antiparallel aligned Fe-Mn-Pt based SAF structure, irradiated by a fs laser with a fluence of 330 μJ cm^{-2}. (b) THz waveforms measured from the Fe-Mn-Pt based SAF structure in the absence of an external field (solid red line) and under an applied field, H = 200 Oe (dashed green line). Additionally shown is the emission from an equivalent, single layer, Fe-Mn-Pt (5 nm) ferromagnet under a positive applied field (dotted black line). Images have been reproduced with permission from Zhang *et al.*[143]

THz emitters commonly used in THz-TDS		Key characteristics desired in a THz emitter			
		Electric field > 100 kV/cm	Bandwidth > 10 THz	Gapless spectral coverage over 0.1 - 10 THz	Photoexcitation with nJ - pulse energies
PCAs	GaAs	✓ R1	✓ R2	×	✓ R3
	InGaAs	×	×	×	✓ R4
Inorganic Crystals	ZnTe	×	✓ R5	×	✓ R6
	GaP	×	×	×	✓ R7
	$LiNbO_3$	✓ R8	×	×	×
Organic Crystals	DAST	✓ R9	✓ R10	×	✓ R11
	DSTMS	✓ R12	✓ R13	×	✓ R14
	OH1	✓ R15	✓ R16	×	×
	Air plasma	✓ R17	✓ R18	✓ R19	×
	Spintronic	✓ R20	✓ R21	✓ R22	✓ R23

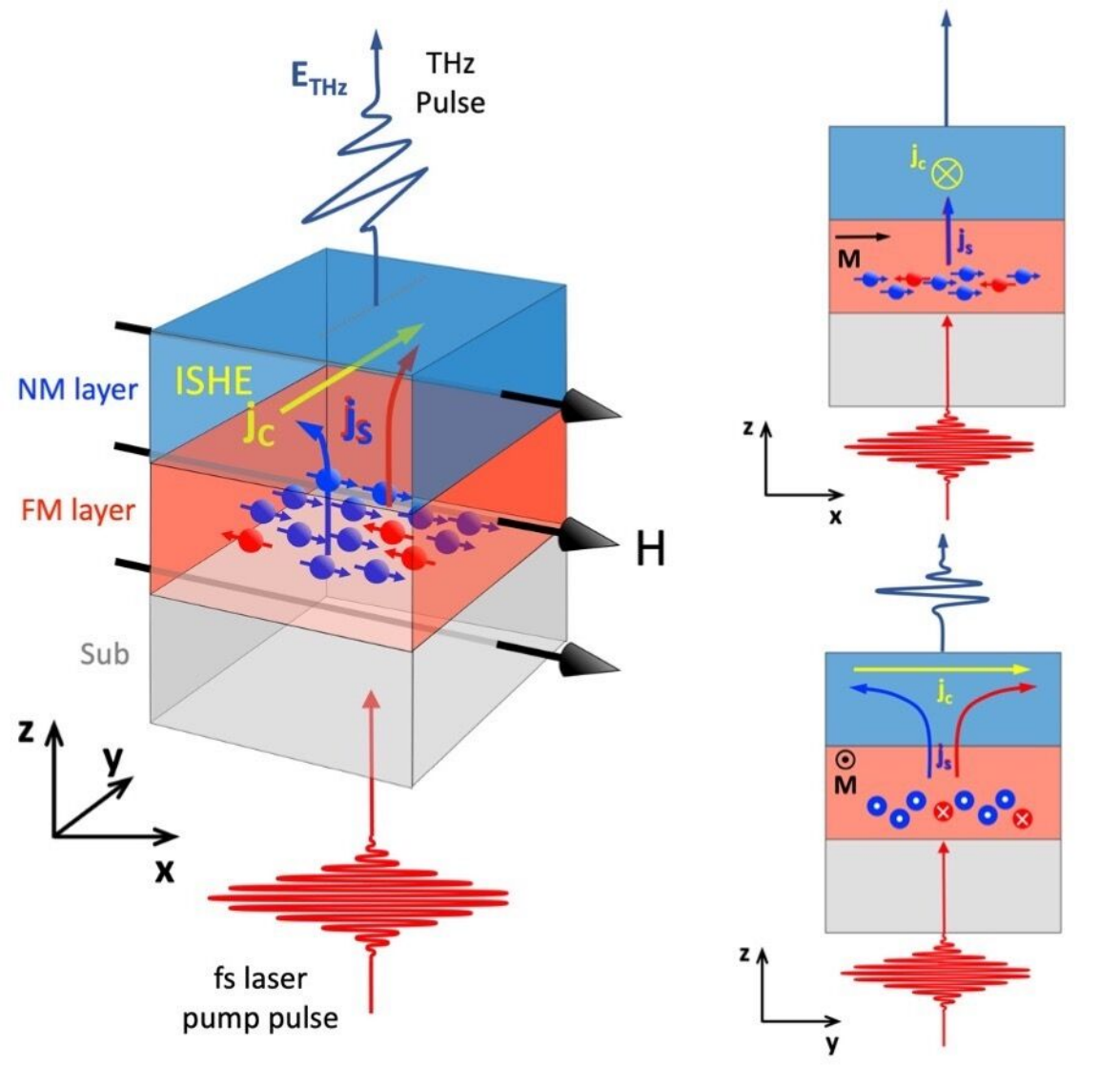
E_THz
THz
Pulse
NM layer
ISHE
j_c
j_s
FM layer
H
Sub
z
y
x
fs laser
pump pulse
j_c
M
j_s
z
x
j_c
j_s
M
z
y

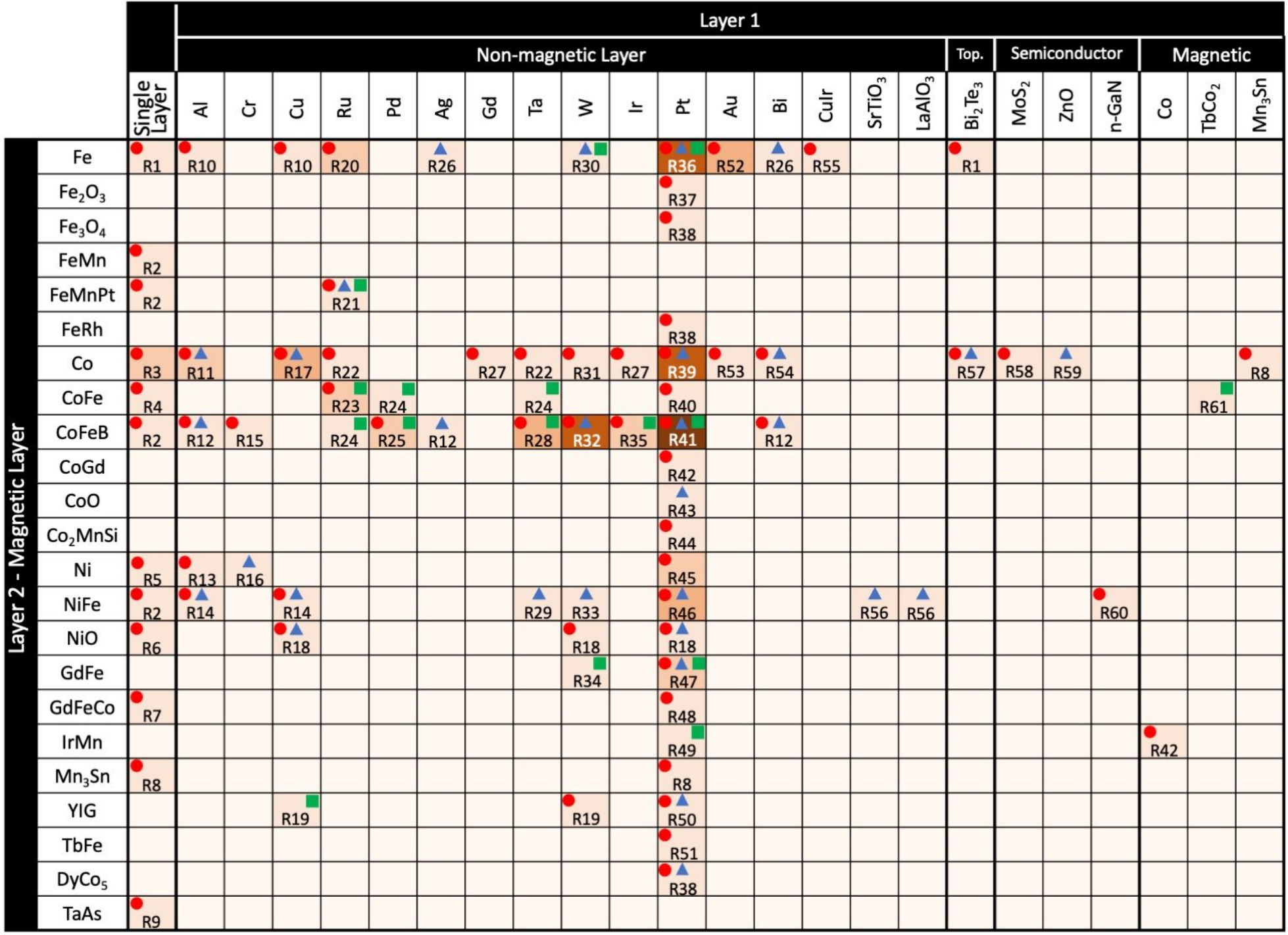
Layer 1
Non-magnetic Layer
Top.
Semiconductor
Magnetic
Single Layer
Al
Cr
Cu
Ru
Pd
Ag
Gd
Ta
W
Ir
Pt
Au
Bi
CuIr
$SrTiO_3$
$LaAlO_3$
Bi_2Te_3
MoS_2
ZnO
n-GaN
Co
$TbCo_2$
Mn_3Sn
Layer 2 - Magnetic Layer
Fe
Fe_2O_3
Fe_3O_4
FeMn
FeMnPt
FeRh
Co
CoFe
CoFeB
CoGd
CoO
Co_2MnSi
Ni
NiFe
NiO
GdFe
GdFeCo
IrMn
Mn_3Sn
YIG
TbFe
$DyCo_5$
TaAs
15+
10-14
5-9
3-4
1-2
0
bilayer
trilayer
multilayer